Volume 18
Number 9
7 May 2025
Pages 3873–4482

Energy & Environmental Science

rsc.li/ees

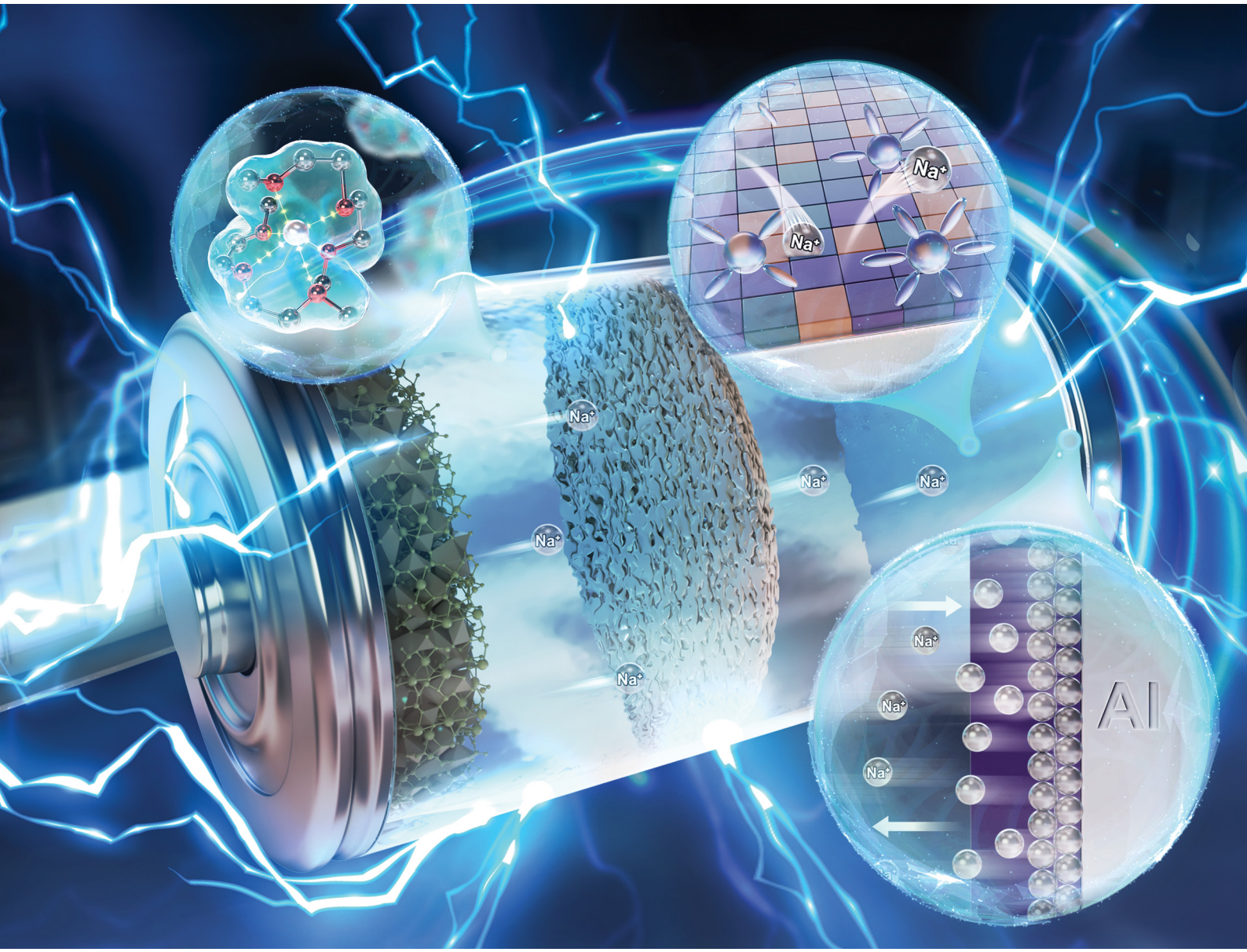

ISSN 1754-5706

ROYAL SOCIETY OF CHEMISTRY

REVIEW ARTICLE
Minghua Chen, Huang Zhang, Stefano Passerini *et al.*
Anode-free sodium metal batteries: optimisation of electrolytes and interphases

Energy & Environmental Science

ROYAL SOCIETY OF CHEMISTRY

REVIEW

View Article Online
View Journal | View Issue

Cite this: *Energy Environ. Sci.*, 2025, **18**, 3887

Anode-free sodium metal batteries: optimisation of electrolytes and interphases

Huihua Li,†[a] Fanglin Wu,†[b] Jian Wang, †[c] Jingxuan Wang,[a] Hongxu Qu,[a] Minghua Chen, *[a] Huang Zhang *[a] and Stefano Passerini *[cd]

Received 8th January 2025,
Accepted 3rd March 2025

DOI: 10.1039/d5ee00136f

rsc.li/ees

Anode-free sodium metal batteries (AFSMBs) represent a significant advancement in energy storage technology, offering high energy density and cost-effective solutions. However, their applications are impeded by the critical sodium deposition behavior, which poses safety risks and compromises battery performance. This review examines the recent progress in electrolyte and interphase optimization which is pivotal for the realization of dendrite-free sodium anodes in AFSMBs. We elucidate the mechanisms of sodium deposition, dendrite formation, and their impacts on battery performance, with the focus on electrolyte composition. A stable solid electrolyte interphase (SEI) is emphasized for preventing dendrite growth and improving Coulombic efficiency (CE). Also, recent strategies in interfacial design, such as the introduction of artificial SEI layers, the architectural design of current collectors, and the electrochemically interfacial kinetic modulations which have shown a great promise in regulating sodium deposition and enhancing battery performance are presented. Lastly, an outlook on the challenges and future directions is provided for achieving safer AFSMBs that are more durable, and capable of delivering higher energy densities, thereby facilitating their integration into practical applications.

Broader context

The global transition towards sustainable energy sources and the increasing demand for efficient energy storage systems need innovative battery technologies. Anode-free sodium metal batteries (AFSMBs) offer significant advancements in terms of energy density and cost-effectiveness compared to traditional lithium-ion batteries, making them a promising candidate for next-generation energy storage systems. However, their practical application is currently hindered by issues such as dendrite growth and low Coulombic efficiency, which lead to safety concerns and reduced battery life. This review underscores the importance of optimizing electrolytes and interphases to enhance the stability and performance of AFSMBs. By focusing on the formation of a stable solid electrolyte interphase (SEI) and controlling sodium deposition, this work contributes to a progressive understanding of the electrolyte and interfacial chemistry in AFSMBs. This understanding provides a crucial foundation for the further development of advanced sodium batteries, promoting a more sustainable energy technology and supporting the broader goal of integrating renewable energy into the grid.

1. Introduction

The continuous consumption of fossil fuels has resulted in urgent concerns regarding global climate change and the energy crisis. The implementation of renewable energy sources such as wind and solar power has accelerated over the past few years.[1] However, the generation of these renewable energy sources is characterized by inherent intermittency and unpredictability. Therefore, developing cost-effective and reliable energy storage technologies is necessary to efficiently modulate the timing and location of electric energy generation and consumption. Lithium-ion batteries (LIBs), commercialized in the 1990s, have greatly influenced the transformation of modern society.[2] With the merits of high energy conversion efficiency, long lifespan, low maintenance cost, and small compact size, currently, LIBs dominate the market for portable electronics and electric vehicles (EVs). However, the widespread application of LIBs is threatened by the price fluctuation of raw materials due to the growing market demand for large-scale energy storage

[a] *Key Laboratory of Engineering Dielectric and Applications (Ministry of Education), School of Electrical and Electronic Engineering, Harbin University of Science and Technology, Harbin 150080, P. R. China. E-mail: zhang.huang@hrbust.edu.cn, mhchen@hrbust.edu.cn*
[b] *State Key Laboratory of Advanced Technology for Materials Synthesis and Processing, Wuhan University of Technology, Wuhan 430070, P. R. China*
[c] *Karlsruhe Institute of Technology, Helmholtz Institute Ulm (HIU), Helmholtzstrasse 11, D-89081 Ulm, Germany. E-mail: stefano.passerini@kit.edu*
[d] *Austrian Institute of Technology (AIT), Center for Transport Technologies, Giefinggasse 2, 1210 Wien, Austria*
† These contributed equally to this work.

systems as well as the scarcity and uneven distribution of lithium (Li) reserves.[3,4]

Sodium (Na) is a cost-effective alternative charge carrier for electrochemically storing electrical energy in batteries.[5] From a practical perspective, sodium can be easily obtained from sodium chloride (NaCl), sodium sulfate (Na_2SO_4), and sodium carbonate (Na_2CO_3), which occur naturally in seawater, brine, and minerals.[6] As a result, it is unlikely to be affected by cost fluctuations and limited supply. In addition, Na and Li belong to the same group (group IA) meaning the existing operating principles of LIBs are suitable for the development of sodium-ion batteries (SIBs). In terms of current collectors, copper current collectors can be replaced with lighter and cheaper aluminum for the anode, since sodium does not alloy with aluminum at low potential.[7] However, conventional SIBs possess the following drawbacks: (1) graphite, the most commonly used commercial anode material in LIBs, does not efficiently host sodium ions.[8,9] Although extensive efforts have been dedicated to screen promising Na anode materials, such as metal oxides, sulfides, phosphides,[10,11] and metal alloys,[12] the necessary modification for performance enhancements require extremely high-cost nano-engineering due to their relatively high redox potentials and severe volume change; (2) sodium ions possess larger ionic radius (Na, 1.02 Å) and higher atomic weight than those of Li ions,[13,14] leading to lower volumetric and gravimetric energy density. These issues render SIBs with a very low specific energy of $\sim$150 W h kg^{-1}, *i.e.*, about half that of LIBs.[15,16] Therefore, to mitigate these inherent limitations, sodium metal batteries (SMBs) are being considered as competitive candidates for practical applications.[17,18]

Sodium as metal anode in SMBs offers high theoretical capacity (1166 mA h g^{-1}) and low redox potential (-2.71 V *vs.* standard hydrogen electrode (SHE)).[13,19,20] However, SMBs usually need a large amount of sodium metal as the anode to compensate for the electrode capacity loss, which raises safety concerns and hinders further increase of the energy density. The concept of anode-free (rechargeable) SMBs (AFSMBs) has been introduced to address this issue of excess Na for sodium metal chemistry (Fig. 1a). Ideally, a bare current collector, *i.e.*, copper or aluminum foil, is used as the Na metal deposition substrate in combination with a sodiated cathode material, introducing the following advantages (Fig. 1b): (i) the absence of excess sodium metal increases the volumetric and gravimetric energy densities of cells while reducing the inherent safety issues; (ii) the fabrication of the AFSMBs integrates well with existing battery production procedures, decreasing troublesome re-customization and device calibrations; (iii) costs and energy consumption would be reduced due to unnecessary production of Na metal, as well the coating, drying and maintenance of the anode electrodes. These advantages support the feasible development of Na anode-free batteries, as reflected by the recent surge of publication numbers (Fig. 1c).

Similar to anode-free lithium metal batteries, AFSMBs also encounter limitations on the anode side related to side reactions, severe volume change, dead sodium, and dendrite growth during the repeated sodium deposition-dissolution processes, which may lead to performance degradation and even cell failure, especially considering the high reactivity of Na metal.[17,21] Moreover, sodiated cathodes are the only Na source for the formation of sodium metal on inert current collectors, which would be inevitably consumed due to the formation of the solid electrolyte interphase (SEI), inactive dead sodium and dendrites. Without additional Na inventory to compensate for these

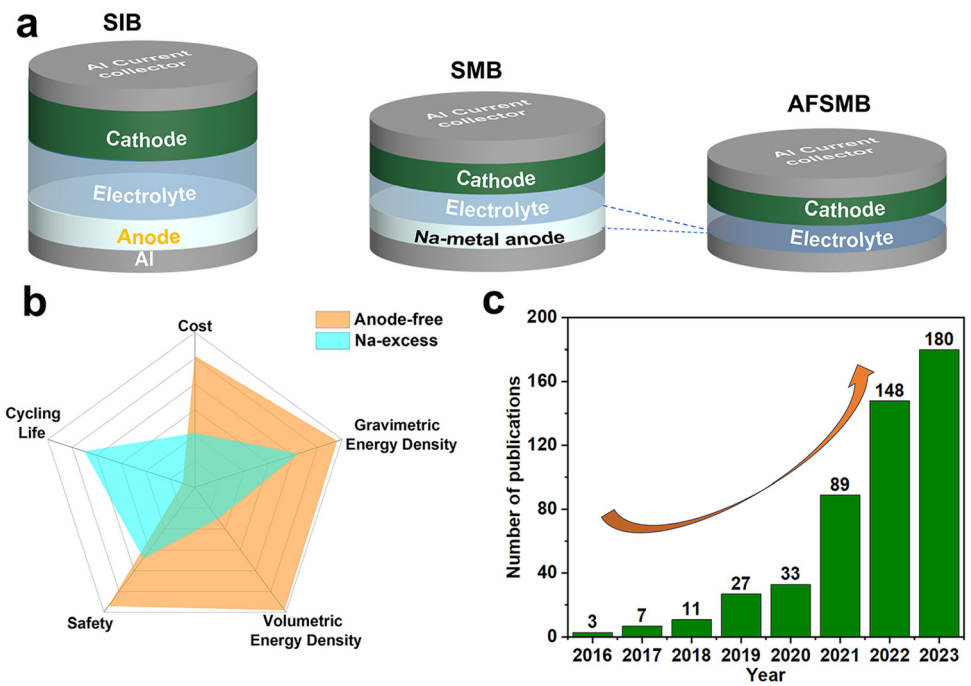

Fig. 1 (a) Schematic representation of different cell models. (b) Radar plot presents the weaknesses and strengths of Na-excess batteries and anode-free batteries. (c) Number of publications from 2016 to 2023 found using the keyword search on anode-free sodium batteries in the "Web of Science" database.

irreversible Na losses, AFSMBs would suffer from rapid initial capacity loss and poor cycle life.[22–24] Therefore, efficiently utilizing the Na ions from the cathode is the key step to advance the overall performance of AFSMBs.[25] This requires the selection of an appropriate electrolyte. Ester- or ether-based solvent used in conventional organic electrolytes would be reduced on the metal anodes before deposition, inducing by-products formation.[26] In this context, the interface between the electrolyte and current collectors plays a crucial role in determining the reversibility of Na plating/stripping, and its optimization requires appropriate strategies which can be developed only upon elucidation of the mechanism.[27]

Recently, efforts have been devoted to optimize the long-term cycling stability of AFSMBs, as summarized in Fig. 2. These include (i) optimization of the electrolyte formulation to generate reliable SEI;[22,28] (ii) artificial interface designs of the substrate to guide the deposition of sodium;[29,30] (iii) current collector architectures to reduce the local current density of deposition and buffer the volume change over cycling;[23,24,29] (iv) addition of Na compensation source from the cathode;[31,32] and (v) electrochemical protocol optimization to favour plating behaviors.[31,33] Considerable performance improvements of AFSMBs have been achieved tracking the developments of LMBs, but the underlying mechanisms remain unclear, the main difficulty lies in the application of specific measures for SMBs. For example, electrolytes are vital for the performance and stability of anode-free SMBs, as they facilitate Na^+ ion transport, form the SEI, and influence the reversibility of Na metal deposition, significantly impacting cycling stability, efficiency, and safety. However, the typical electrolyte formulation in anode-free LMBs cannot be extended directly into the sodium systems, due to the larger size and lower Lewis acidity of Na ion, higher reactivity of Na metal, as well as the different solubility and ionic conductivity of sodium salts in electrolytes.[34,35] To enhance the overall performance of AFSMBs, innovation in electrolyte and interfacial chemistries of the systems are requisite.

Herein, an overview of electrolyte developments and their interfacial chemistries affecting the performance metrics of AFSMBs are presented. Specifically, conventional, diluted organic electrolytes in AFSMBs are reviewed. Following, high salt-concentration, co-solvents, and dual-salt electrolyte strategies are considered in terms of improvements on Na metal deposition behaviors and overall electrochemical properties. The electrode/electrolyte interphase on the anode is also discussed as another key factor affecting the Na deposition. Subsequently, the most promising strategies for extending the cycle life are presented with a perspective on the challenges and future research directions for AFSMBs to become a competitive battery technology.

2. Mechanisms and failure factors in AFSMBs

2.1. Principal mechanisms

Conventional rocking-chair SIBs are composed of inert current collectors, a cathode, a separator, and an anode, as illustrated in Fig. 1a.[42] The cathode material is normally a sodium-rich compound, such as a layered transition metal oxide, polyanionic framework, Prussian blue analogue, *etc.* The anode active material for SIBs is usually hard carbon, known as a typical disordered non-graphitic carbon with relatively high surface area and microporous structure.[43] Replacing the hard carbon anodes with metallic sodium, SMB cells can deliver significantly improved energy density, which is comparable to commercial LIBs.[44] In the anode-free configuration, the sodium metal anode is omitted,[42] resulting in AFSMB to exhibit superior performances on energy, cost, safety, and sustainability than LIBs.[45] The charge and discharge processes in AFSMBs are distinct to those of traditional rechargeable rocking-chair batteries (SIB), in which the cathode material is essential for supplying the necessary sodium ions to guarantee the battery's operation, while the optimal Na plating and stripping at the anode current collector is capital for the cell's long-term operation.[38,46]

In AFSMBs, the depositon of sodium on the inert anode current collector during the initial charging induces the heterophase nucleation process. This process, expected to also generate a stable SEI, initiates the battery's operation.[31,46,47] After the initial charge, the AFSMB operates like a traditional SMB, but with restricted Na metal availability upon the following discharge, when the Na^+-ions are re-intercalated into the cathode. In this step, AFSMBs rely solely on the limited deposited sodium.[48] Thus, the key distinction between AFSMBs and standard SMBs lies in the sodium nucleation process due to the difference of substrates for initial nuclei of sodium.[38,49]

In theory, the nucleation of Na is determined by the Gibbs free energy, which is a function of the sodium ion concentration in the electrolyte near the electrode. The driving force for Na metal plating results from the Gibbs energy drop when the electrolyte changes from supersaturation to saturation at the electrolyte–electrode interface. The size of sodium nuclei is related to overpotentials, with higher overpotentials leading to smaller nuclei. Small nuclei and irregular shapes can speed up the formation of the solid SEI layer and cause faster depletion of the electrolyte due to the larger surface area.[50] During the sodium nucleation process, many nuclei form evenly on the current collector's surface. After nucleation, sodium metal grows on these nuclei, with new sodium ions preferentially reducing onto the initial nuclei, leading to larger structures, as illustrated in Fig. 3a.[51] During the growth process, the initial sodium nuclei's morphology can transform into various shapes, including needle-like, spherical, or columnar forms. This transformation is contingent upon factors such as electrolyte composition and the conditions under which deposition occurs. The SEI that forms on the diverse sodium morphologies exhibits varying properties, inevitably affecting the Na deposition behaviours due to the necessity for Na^+ ions to penetrate the SEI layer and transfer electrons from the substrate to achieve sodium reduction and subsequent growth. Hence, the precise control over the morphology of the deposited sodium and the SEI layer is pivotal for optimizing cell performance, ensuring both efficiency and durability of the battery.

2.2. Critical challenges in AFSMB

Unlike traditional SMBs with excess Na, the electrochemical performance of AFSMBs is predominantly constrained by the

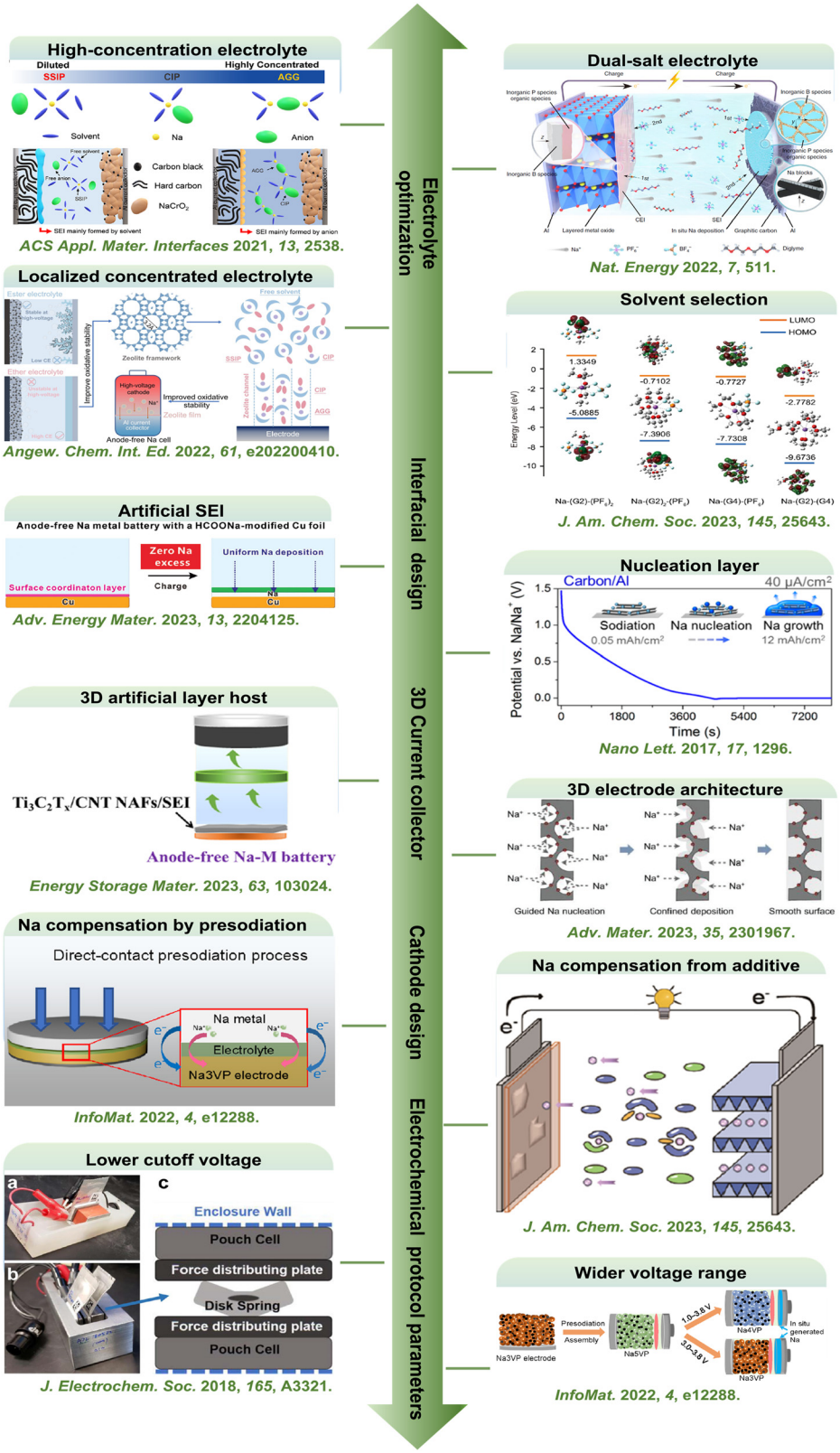

Fig. 2 Current research trends in AFSMBs. High-concentration electrolyte. Reproduced with permission.[36] Copyright 2021 American Chemical Society. Localized concentrated electrolyte. Reproduced with permission.[22] Copyright 2022 Wiley-VCH GmbH. Dual-salt electrolyte. Reproduced with permission.[37] Copyright 2022 Nature Publishing Group. Solvent selection. Reproduced with permission.[32] Copyright 2023 American Chemical Society. Nucleation layer. Reproduced with permission.[38] Copyright 2017 American Chemical Society. Artificial SEI. Reproduced with permission.[39] Copyright 2023 Wiley-VCH GmbH. 3D artificial layer host.[40] Reproduced with permission.[40] Copyright 2023 Elsevier. 3D electrode architecutre. Reproduced with permission.[41] Copyright 2023 Wiley-VCH GmbH. Na compensation by presodiation. Reproduced with permission.[31] Copyright 2022 Wiley-VCH GmbH. Na compensation from additive. Reproduced with permission.[32] Copyright 2023 American Chemical Society lower cutoff voltage. Reproduced with permission.[33] Copyright 2018 The Electrochemical Society. Wider voltage range. Reproduced with permission.[31] Copyright 2022 Wiley-VCH GmbH.

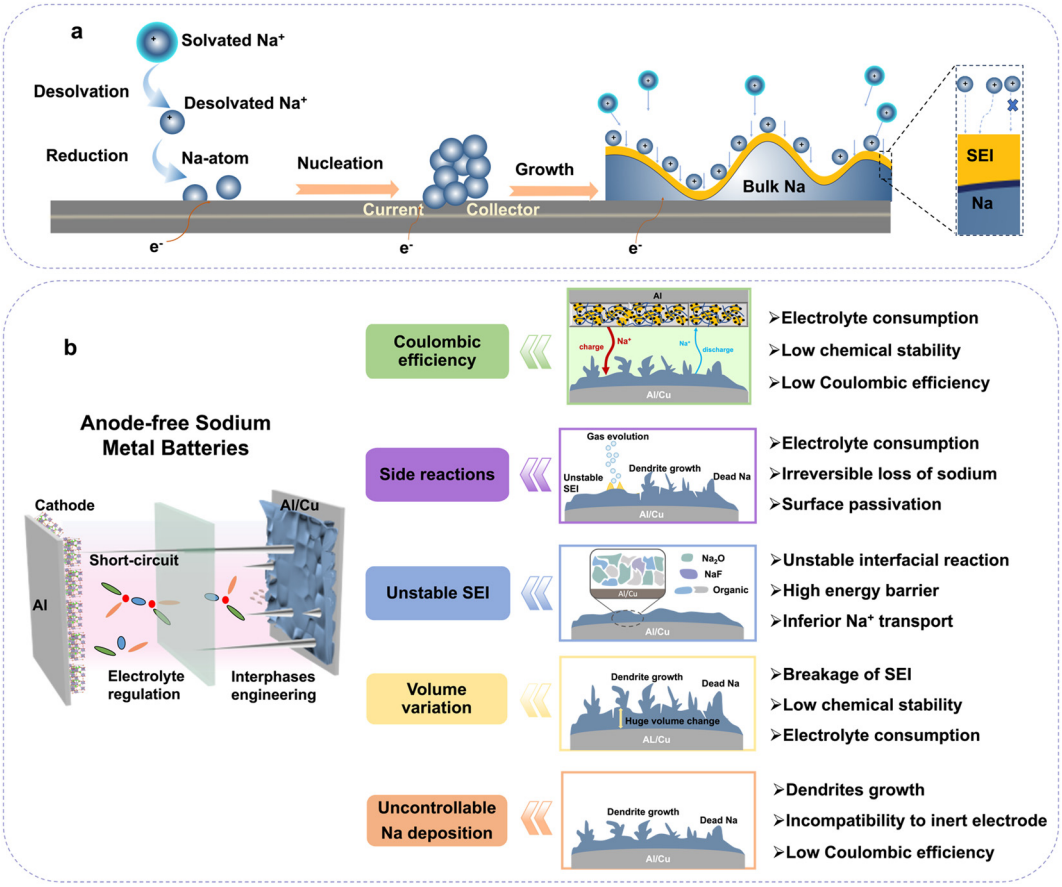

Fig. 3 (a) Processes involved in the Na deposition on an inert current collector. (b) Summary of the electrolyte and interphase challenges of anode-free Na metal batteries.

efficiency of sodium deposition and stripping due to the limited available Na^+ ions. The primary causes of performance degradation in AFSMBs include the inevitable side reactions of the electrolytes, resulting in low CE, and the increasing overpotential associated with the random deposition of metallic Na on the current collectors. Irreversible electrochemical reactions within AFSMBs, such as the electrolyte decomposition, the generation of the SEI, the growth of Na dendrites, and the formation of dead sodium, accelerate the capacity decay. Gaining insights into the fate of these Na^+ ions and elucidating the mechanisms behind capacity decay is imperative for devising strategies to enhance the operational lifespan of AFSMBs. Understanding these factors and their interactions is essential for developing effective optimization strategies to improve the cycling stability and reversibility of AFSMBs. The challenging factors influencing capacity loss are summarized as follows, and concluded in Fig. 3b:

(1) Unstable and irreversible passivation.

Sodium, with a low reduction potential (E_{Na/Na^+}: −2.73 V), is an extremely reactive alkaline metal, which can be easily passivated upon interactions with electrolytes, *i.e.*, forming the SEI.[19] The structural integrity and composition are pivotal in determining the metal electrode performance in batteries.[19,30,52] A robust and thin SEI layer can allow the migration of sodium ions, but prevent the electron transfer to the electrolyte, thereby mitigating its continuous degradation.[53] However, in instances where the SEI layer is suboptimal, the mechanical stress induced by volumetric fluctuations during sodium deposition can favor SEI cracking, resulting in the continuous formation of new SEI layer.[54] This not only accelerates electrolyte consumption and depletes sodium reserves, but also leads to uneven electric field distribution and Na metal deposition, and uncontrollable dendrite growth.[55,56] Consequently, these phenomena can rapidly diminish the battery's CE and capacity retention, underscoring the imperative for an optimal SEI layer in sustaining the longevity and operation of AFSMBs.

(2) Uncontrollable Na deposition.

In AFSMBs, the Na plating directly takes place on the current collector's surface. The energy barriers for sodium nucleation on most inert or hetero current collectors are notably high, implying that a significant overpotential is required to initiate sodium deposition. The initial overpotential can favor non-uniform deposition morphologies,[57] exerting a profound influence on the first deposition step as well as the subsequent stripping process and the pattern of deposition in subsequent cycles.[58] Additionally, non-uniform deposition of sodium can intensify dendritic growth, curtail the active sodium inventory, and culminate in a diminution of the battery's electrochemical performance metrics, such as CE and capacity retention. It is

widely accepted that the limited sodium reservoir in AFSMBs influences the reversibility of the electrochemical process, with a stringent requirement for a Na plating/stripping CE above 99.9% to ensure that the battery can retain 80% capacity over 200 cycles.[57,59]

(3) Side reaction and volume variation.

The irregular initial deposition of sodium and an unstable, defective SEI layer can induce the proliferation of Na dendrites,[60] which amplifies the electrolyte-sodium contact area, foster side reactions and electrolyte's depletion. Persistent side reactions at the interface of sodium dendrites and the electrolyte might favor the creation of dead sodium, encapsulated by the SEI layer.[61,62] Additionally, sodium deposits that are subjected to ongoing dendritic growth may evolve into a porous structure, leading to substantial volumetric fluctuations during the plating and stripping processes.[61] This dendritic expansion remarkably reduces the availability of sodium that actively participates in electrochemical reactions, resulting in an irreversible loss of sodium and increased electrolyte consumption. Consequently, this chain of events diminishes CEs, degrades capacity retention, and shortens the cycle life of the battery. These challenges primarily arise from fundamental problems in the sodium plating/stripping processes, particularly during the deposition. Thus, building upon the foundational knowledge of the challenges faced by AFSMBs, the development of AFSMBs can be directed towards achieving higher efficiency, lifespan, and safety, facilitating their integration into a wider range of energy storage solutions.

3. Electrolyte engineering in regulating current collector/electrolyte interface

Transferring the limited sodium source from the cathode to the anodic current collector is a pivotal process in the operation of AFSMBs. The electrolyte, acting as the conduit for the movement of charge-carrying ions between electrodes, exerts significant influence over the battery's electrochemical reactions during cycling. It directly impacts sodium metal nucleation and growth, thus, the battery's cycle life and power output.

The stability of AFSMBs through repeated cycles is largely governed by the SEI layer that forms on the anodic current collector. The quality and composition of electrolytes are paramount in dictating the SEI's characteristics. Generally, a well-designed electrolyte can shape the structure of the deposited sodium metal and mitigate side reactions that deplete the active sodium and electrolyte resources. This, in turn, extends the operational lifespan of AFSMBs. Therefore, the achievement of high-performance electrolytes is crucial for the advancement of AFSMBs, while the optimization of electrolytes for AFSMBs is a complex process that requires a careful balance of solvents, salts, salt concentrations, multi-salt blending, and additives. Each of these elements contributes to the formation of a stable SEI layer, which is paramount for the high-performance and longevity of AFSMBs. In the following, the specific optimisation strategies of electrolytes for AFSMBs will be discussed.

3.1. Conventional organic liquid electrolytes

Conventional, dilute liquid electrolytes can be classified into three groups based on solvent chemistries: (i) ether-based, such as methoxymethane (DME), diethylene glycol dimethyl ether (DEGDME) and tetraethylene glycol dimethyl ether (TEGDME), and 1,3-dioxolane (DOL); (ii) ester-based, such as diethyl carbonate (DEC), ethylene carbonate (EC), dimethyl carbonate (DMC), and propylene carbonate (PC); and (iii) ionic liquids. The application of these solvents vary significantly owing to their intrinsically different physical and chemical properties, which play a pivotal role in shaping the battery's performance (Table 1).[63,64] For instance, ether-based solvents are favorable for their elevated dielectric constant, which promote ion dissociation and improve ionic conductivity. Ester-based solvents offer superior electrochemical stability and reduced propensity for side reactions with electrode materials, thereby fostering a more robust and enduring SEI layer. However, utilizing carbonate-based electrolytes in AFSMBs often leads to significant side reactions with sodium metal, accompanied by gas evolution. These reactions impede the formation of a stable SEI on the anode current collector, as observed through optical microscopy by Pfeifer *et al.*[65,66] In contrast, ether-based solvents have been found to form more stable inorganic layers on the anode current collector, contributing to CE exceeding 99.9%.[19,67] As a result, the majority of liquid electrolyte-based AFSMBs reported in the literature involve ether-based solvents because of their propensity to inhibit the growth of lithium dendrites.[68–70]

Within the anode materials innovation, ester-based electrolytes have attracted significant research interest due to their efficacy in forming protective SEI on carbonaceous anodes.[71,72] Yet, as the cells endure more than a hundred cycles, the risk of metallic dendrite-induced short circuits remains, suggesting that these electrolytes are still not enduring against long-term dendrite proliferation. A revival of interest in ether-based electrolytes for SIBs is propelled by the compelling discovery that sodium ions are capable of co-intercalating into the graphite structure when paired with ether-based solvent molecules.[73–77] In this context, the utilization of ether-based electrolytes has been expanded to facilitate the improvement of sodium metal anodes, enabling the formation of a homogenous and robust SEI which can effectively suppress the growth of sodium dendrites and improve long-term reversibility.[78,79] Cui's group highlighted a dilute glyme-based electrolyte containing 1 M $NaPF_6$ for a prolonged, non-dendritic sodium-metal anode at room temperature.[79] The formation of stable inorganic SEI films enriched in Na_2O and NaF were observed in the glyme-based electrolytes (mono-, di-, and tetraglyme), whereas such inorganic components-rich films were not generated in ester-based electrolytes. This suggests that ether-based electrolytes have the ability to form highly stable passivating inorganic layers on the sodium metal surfaces, enabling dendrite-free sodium plating in batteries.[67] This versatility of glyme-based electrolytes extends to various salt systems, offering a promising avenue for enhancing the performance of AFSMBs. By utilizing 1 M sodium tetrafluoroborate ($NaBF_4$) salt into tetraglyme as a

Table 1 Properties of organic solvents used in AFSMB electrolyte systems

	Name	Structure	$T_{m,p}$ (°C)	$T_{b,p}$ (°C)	ε (25 °C)
Ether-based solvents	DME		−138.5	−23	5
	DEGDME	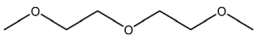	−64	162	7.2
	TEGDME	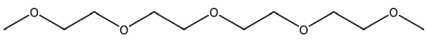	−30	275	7.5
	DOL		−95	74	7.3
Ester-based solvents	DEC	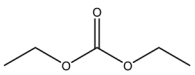	−74.3	126	2.8
	EC	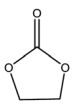	36.4	248	89.8
	DMC	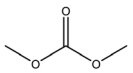	4.6	91	3.1
	PC	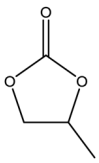	−48.8	242	64.9

dilute electrolyte, a highly reversible Na plating/stripping process on Cu substrate was realized. As a result, $Na_2Fe_2(CN)_6$//Cu AFSMBs exhibited a commendable capacity retention of 76% after 100 cycles.[80] The improved reversibility of the sodium metal anode in ether-based electrolytes can be attributed to its high compability with metal anode at low potential, favoring the formation of a robust NaF and Na_2O-dominated SEI as a protective layer and electronic insulator, effectively preventing the electrolyte from continuously reacting with the reactive sodium metal plated on the Cu, and promoting uniform sodium deposition. Meanwhile, the distinctive solvation characteristics in ether electrolytes contributes to a significantly reduced activation energy for desolvation, favoring rapid Na^+ transport and ensuring uniform deposition of sodium metal. However, the cyclability of the battery in conventional ether-based electrolyte can be significantly compromised when subjected to elevated voltages, such as up to 4.0 V, which is primarily attributed to the relatively low oxidation potential of the ether solvent. This intrinsic limitation underscores the necessity for further chemical refinement of the electrolyte to enhance its resistance to the oxidative decomposition. Overcoming this challenge is essential for prolonging the battery's operational lifespan and fulfilling its maximum capacity in high-voltage AFSMBs applications.

Ionic liquid electrolytes (ILEs) exhibit exceptional potential for SMBs due to their non-volatility, non-flammability, and wide electrochemical stability windows (>4.5 V *vs.* Na^+/Na), which significantly enhance operational safety and compatibility with high-voltage cathodes.[81,82] The unique solvation properties of ILEs further enable robust SEI formation: anions like FSI^- preferentially decompose to create inorganic-rich, ionically conductive SEI layers,[83,84] while long-aliphatic-chain cations (*e.g.*, $[EMIm]^+$) promote uniform sodium deposition *via* electrostatic shielding effects and lithiophobic interactions.[85] These mechanisms collectively suppress dendrite growth and stabilize sodium plating/stripping, showing an unique promise in sodium batteries. However, challenges such as high viscosity, cost, synthesis complexity, compatibility issues, and limited sodium transference numbers hinder their application.[86,87] In this context, strategies like hybrid electrolytes, eutectic blends, solvation engineering, nucleation layer design, and additive integration can enhance performance. Recently, non-solvating and low-viscosity co-solvents have been used to dilute ionic liquid electrolytes, *i.e.*, locally concentrated ILEs, without disrupting the local solvation structure, were reported, exhibiting lower viscosity, faster ionic transport, and enhanced compatibility toward metal anodes, can be feasible options for the AFSMBs.[88,89]

3.2. Concentrated electrolytes with anion chemistry

The use of high-concentration sodium salt electrolytes has emerged as an advantageous strategy, supplying an ample amount of sodium ions to the system.[90,91] By increasing the concentration of salts in the electrolyte, the evolution of solvation structure in the electrolyte will change, leading to increased cation–anion complexes, such as contact ion pair (CIP) and aggregate (AGG) species.[92,93] These are instrumental in forming a SEI layer derived from anion decomposition, which typically results in a more reliable barrier against electrolyte degradation and sodium dendrite growth.[36,94] Therefore, increasing the salt concentration in ether electrolyte to construct a concentrated electrolyte is an effective approach to expand the oxidative stability window for high voltage cathodes (above 4.0 V), consequently improving the energy density of anode-free batteries. In 2016, the improved performance of a high-concentration DME-based

electrolyte consisting of 4 M LiFSI in anode-free $LiFePO_4$‖Cu battery was pioneeringly reported.[95] The concentrated electrolyte enabled reversible Li plating and stripping, minimizing side reactions. However, the use of concentrated electrolytes in AFSMBs has been rarely reported, even though the current investigation has demonstrated that the elevated concentration in electrolyte promotes the evolution of solvation structure enabling improved oxidative stability.

Furthermore, the induced solvation change enables the formation of an inorganic-rich SEI, which suppress sodium dendrite growth, and accelerate Na^+ desolvation and diffusion kinetics.[96–98] Interestingly, incorporating a mesoporous structure such as metal–organic frameworks (MOFs) at the electrode's surface can generate a quasi-high concentration electrolyte in these confined structures, addressing the low dissolution issue of salts in ether electrolyte. For example, Lu *et al.* developed a zeolite molecular sieve film to produce a highly aggregated solvation structure in the pores and enabled a de-solvation process through the size effect in AFSMB (Fig. 4a).[22] The oxidative stability of ether-based electrolytes was extended from the original 2.5 to 4.5 V *vs.* Na/Na^+ (Fig. 4b), without compromising the Na reversibility of the anode (99.91%). As a result, the unique electrolyte formulation has been demonstrated to support a long lifespan (250 cycles) for 4.0 V-class anode-free cells. These discoveries have prompted a surge of endeavors to explore different electrolyte modifications for AFSMBs.

Similarly, a "liquid-in-solid" electrolyte was designed by confining aggregated liquid ether electrolytes into Na^+-exchanged zeolite molecular sieves.[100] Due to the enhanced interfacial compatibility by the high stability of silica-aluminum oxides host, this electrolyte not only offered high-voltage stability inherent to solid-state zeolite-based electrolytes, but also enabled an ultra-high CE of 99.84% for Na stripping/plating from liquid ether electrolyte. This is achieved by breaking through the Na^+ transport channel of Na-containing zeolite molecular sieves *via* ion-exchange and confining aggregated liquid ether electrolytes within the nanopores and voids of zeolites. The application of this electrolyte in a high-voltage 4.25 V-class AFSMB resulted in an exceptional energy density of 412 W h kg^{-1}, which is comparable to the graphite‖$LiNi_{0.8}Co_{0.1}Mn_{0.1}O_2$ full cells.

The pursuit of highly concentrated electrolytes, aiming to boost oxidative stability and facilitate the interfacial chemistry, still faces notable challenges. As known, the electrochemical plating behavior is closely related to the solvation shell structure of Na^+ in the electrolyte and the local electrode/electrolyte interface. A higher proportion of CIPs and AGGs in solvation structure results in lower energy barriers that need to be overcome, thereby accelerating Na^+ transport and achieving a more uniform distribution. However, a common issue is the increased viscosity characteristic of these solutions, which can restrict ion mobility, resulting in diminished power capability.[101] Furthermore, the use of concentrated Na salts can also result in economic

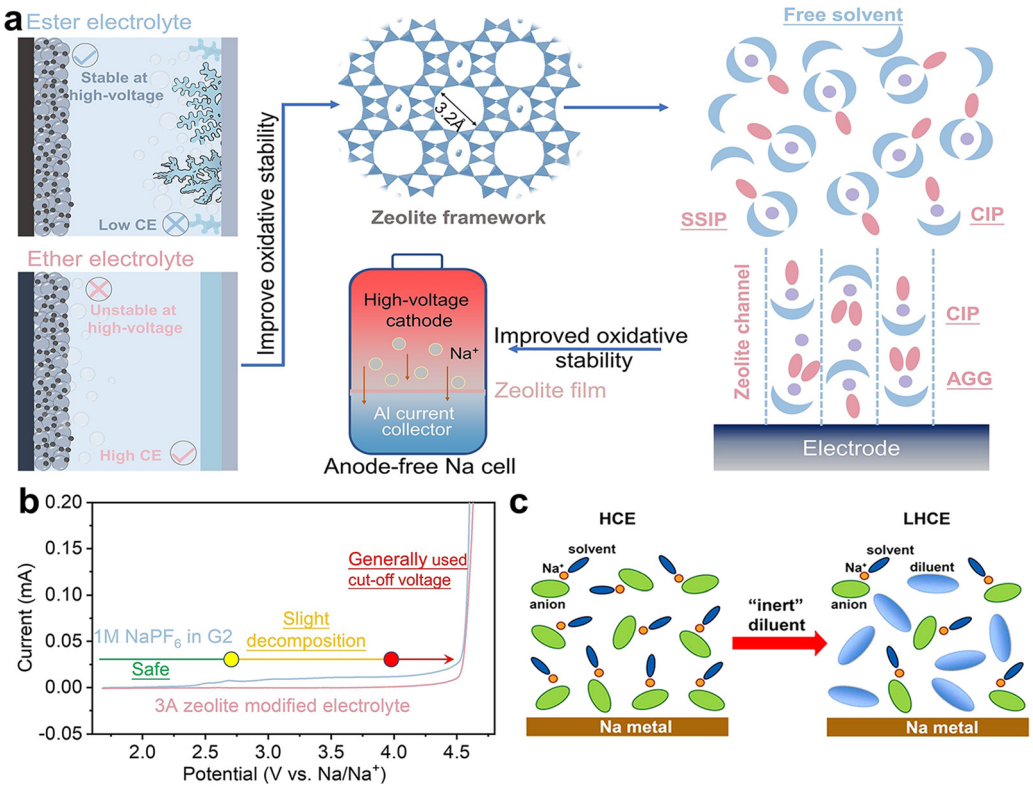

Fig. 4 (a) High-voltage AFSMB assembled by optimizing chemistry aggregation using the 3 Å zeolite molecular sieve. (b) Interpreting the stability of different electrolytes in different voltage regions. Reproduced with permission.[22] Copyright 2022 Wiley-VCH GmbH. (c) Schematic illustration depicting the dilution process from a HCE to a LHCE. Reproduced with permission.[99] Copyright 2018 American Chemical Society.

and applicability concerns. Interestingly, the aforementioned issues can be migrated by diluting the concentrated electrolyte with inert co-solvents, which cannot solvate the ions, which remain in a locally concentrated chemistry. Zheng *et al.* demonstrated that using hydrofluoroether as an inert (non-solvating) diluent can reduce the salt concentration in concentrated electrolytes to below 1.5 M, resulting in a localized high-concentration electrolyte (LHCE). This approach retains the solvation structures typical of highly concentrated electrolytes (HCE, $\geq$4 M) including sodium bis(fluorosulfonyl)imide (NaFSI) and ether solvents, as schematically illustrated in Fig. 4c.[99] The inert diluent has a minimal impact on the anion-involved solvation structure that is typical in concentrated electrolytes. It effectively reduces the concentration of sodium salts, which in turn lowers the viscosity of the electrolyte, enhances its ionic conductivity, and improves its wettability. This innovative strategy of using hydrofluoroethers as diluents to create LHCE environments represents a significant step forward in the development of advanced electrolyte systems for AFSMBs, addressing the challenges of high concentration while optimizing the electrolyte's overall performance.

3.3. Co-solvent electrolyte with solvent chemistry

Ether-based electrolytes, which show a high compatibility with Na metal anodes,[22,24] are thus highly utilized in AFSMBs. To realize their full potentials, it is crucial to extend the voltage window of ether-based electrolytes, allowing for greater oxidative stability and broader applicability in battery systems. Recently, considerable attention has been focused on the development of co-solvent electrolyte systems, offering a promising approach to create cost-effective electrolyte solutions for AFSMBs. It has been reported that the presence of co-solvent can tune the solvation structure with increased participation of anions, which can promote the formation of anion-derived SEI layer and minimize the SEI dissolution.[102,103] In AFSMBs, an electrolyte consisting of 1 M $NaPF_6$ in a solvent mixture of diethylene glycol dimethyl ether (G2) and tetraethylene glycol dimethyl ether (G4) was proposed to enable the operation of P2-/O3-type layered oxide cathodes.[32] The binary electrolyte can facilitate the dendrite-free Na plating/stripping on a carbon coated Al foil and improve tolerance against high-voltage cathode, due to the unique Na^+ solvation structure in G2 (main solvent) and the theoretically low highest occupied molecular orbital (HOMO) energy of G4 (cosolvent), as shown in Fig. 5a and b. When G4 was introduced into the $NaPF_6$/G2 electrolyte, two new solvation structure of Na–(G2)–(G4) and Na–(G4)–(PF_6) were formed, in which the Na–(G2)–(G4) solvent-separated ion pair has the lowest LUMO/HOMO energy, indicating a higher oxidative stability of the optimal co-solvent-based electrolyte. By precisely tuning the chemical composition (Fig. 5c), as the proportion of G4 in the G2/G4 solvent mixture rises from 0 to 20 vol%, there is a continuous increase in the molar percentages of Na–G2–$(PF_6)_2$ and Na–(G2)–(G4) within the overall solvent structures. In the optimal electrolyte with G2 and G4 in the 9 : 1 volume ratio, an inorganic-rich SEI on the current collector was detected after cycling, which effectively regulated the electroplating morphology of Na metal and passivated the surface, as depicted in Fig. 5d. Consequently, anode-

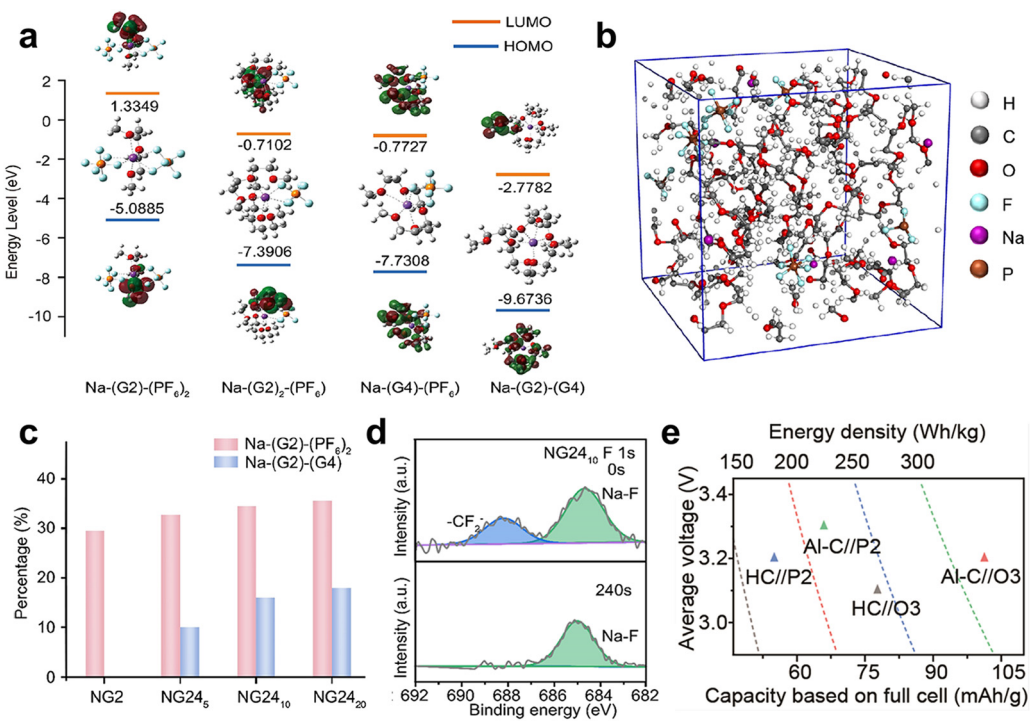

Fig. 5 (a) Cation solvation structures of the hybrid electrolyte (NG2 and NG24) and the energy of their frontier molecular orbitals. (b) Molecular dynamics simulation snapshot of the $NG24_{10}$ electrolyte. (c) Mole percentage of Na–G2–$(PF_6)_2$ and Na–(G2)–(G4) structures in G2/G4 mixture as a function of G4 volume percentage. (d) *Ex situ* XPS F 1s spectra of (d) $NG24_{10}$ collected (before and after Ar^+ etching) from the Al–C collector. (e) Energy density of different full cells. Reproduced with permission.[32] Copyright 2023 American Chemical Society.

free cells in this electrolyte demonstrated a specific energy exceeding 300 W h kg^{-1} in cell level with high CE and long cycle life (Fig. 5e).

In the context of co-solvent electrolytes, solvation structures are also crucial for the interfacial kinetics of Na^+ and significantly dictate the electrochemical performance of AFSMBs. As another competitive co-solvent, the introduction of weakly solvating co-solvents in electrolytes is expected to decrease the coordination of Na^+ with the solvent, while enhancing the ratio of anions in the solvation sheath, which offers a straightforward method to reduce desolvation barriers, thus facilitating desolvation. However, the weakened dissociation of sodium salts in the presence of weakly solvating co-solvents can lead to limited ionic conductivities, presenting a challenge to achieving the necessary balance for high-performance batteries.

Recently, nonfluorinated weakly solvating solvents have been widely employed in electrolytes to improve the reversibility of metal anode, presenting a new direction to design advanced co-solvent electrolyte with wide temperature range for AFSMBs.[104,105] Although the cyclic ether molecules are often excluded from electrolyte formulations, due to their propensity to engage in cationic polymerization when in contact with inorganic salts, 1,3-dioxolane (DOL) as a conventional fluorine-free ether solvent with weakly solvating ability, has been widely used in batteries.[106] Hu *et al.* utilized the DOL as co-solvent to prepare a low-concentration glyme-based electrolyte (0.4 M $NaPF_6$–G2/DOL), in which the DOL can significantly disrupt the cation–anion and solvent–solvent interactions, enabling the fast transport of Na^+ ions in the electrolyte.[107] Moreover, the integration of DOL molecules into the solvation sheath weakened the binding energy between Na^+ and G2 and influenced the energy level distribution around the PF_6^- anions, leading to the low energy barrier for desolvation and enhanced anion-derived interfacial chemistry under relatively low concentrations (Fig. 6a). As proven by the theoretical investigation (Fig. 6b), the solvation complexes in the DOL-diluted electrolyte exhibit a lower lowest unoccupied molecular orbital (LUMO) energy level of −0.36 eV compared to −0.01 eV in the pristine 0.4 M $NaPF_6$–G2 electrolyte, with the Na^+ ions predominantly distributed around PF_6^- within the solvation complex. Consequently, the anion-induced thin SEI, rich in inorganic species such as NaF with high ionic conductivity and Young's modulus, was formed on the current collector, which resulted in high Na plating/stripping CE beyond 99.9% even at low temperature of −55 °C (Fig. 6c and f). In contrast, the surface topography image of the anode cycled in pristine G2 solvent shows a much higher roughness of 17.1 nm (Fig. 6d), and the average Young's modulus was determined to be 0.3 GPa, which is notably lower than the value of 1.1 GPa obtained in the G2/DOL

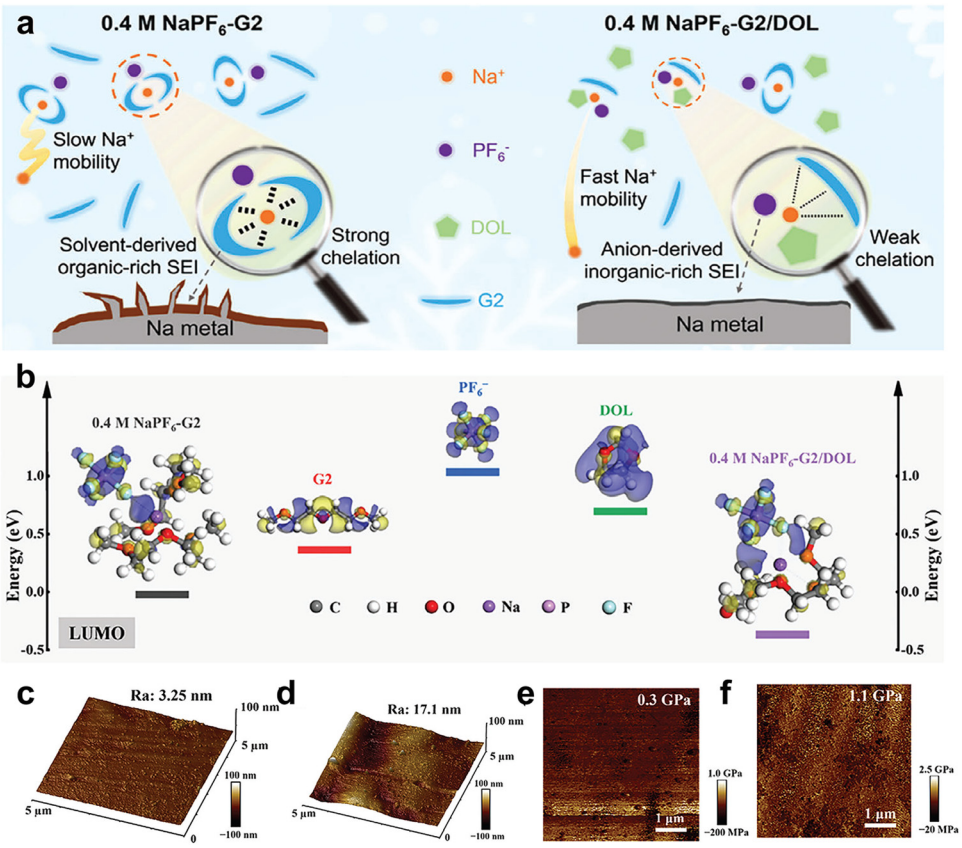

Fig. 6 (a) Schematic diagram of the mechanism of improved Na reversibility by the DOL-diluted electrolyte at low temperature. (b) LUMO of sodium salts, solvent molecules, and solvate complexes in electrolytes. AFM surface profiling of SEI formed in the (c) G2/DOL and (d) pristine G2 electrolytes at −25 °C. Young's modulus mapping of SEI formed in the (e) G2/DOL and (f) G2 electrolytes at −25 °C. Reproduced with permission.[107] Copyright 2024 Wiley-VCH GmbH.

system (Fig. 6e). Accordingly, a 1 A h-capacity pouch cell demonstrated excellent retention of 95% of its initial discharge capacity over 100 cycles at −25 °C. These results indicate that the strategic formulation of solvents in electrolytes offers promising advancements for performance improvement of AFSMBs, which can synergistically affect the Na^+-ion conductivity, desolvation behavior and preferential decomposition of anions.

3.4. Dual-salt electrolyte with anion-interaction chemistry

Besides the solvent chemistry, the inherent nature of salts will also impact the properties of electrolytes and thus the performance of batteries. The tunability of sodium salts is also a key aspect of electrolyte engineering.[108] Similar to the co-solvent systems, mixing different kinds of salts can create an electrolyte with "cock-tial" properties that may influence the solvation ability, tailoring the interfacial chemistries.[109,110]

$NaPF_6$, a typical Na salt, has been widely adopted in stabilizing sodium metal anode by supporting the formation of a desirable solvation structure and SEI.[79,111,112] The mild interaction between Na^+ cations and PF_6^- anions facilitates the dissociation in electrolytes, which enables the high ionic conductivity and ion transference number. Crucially, the PF_6^- anions also participate in the outer solvation structure, and can undergo a preferential decomposition to generate a thin, inorganic-rich SEI, ensuring electrode/electrolyte interfacial stability without continuously consuming electrolytes.[113] In this context, dissolving the $NaPF_6$ in diglyme electrolyte is expected to be a good match for AFSMBs.

It has been reported that the use of $NaBF_4$ in tetraglyme-based electrolyte demonstrated superior stability with Na metal and extended excellent electrochemical window up to 4.2 V.[114] Further incorporating the $NaBF_4$ salt into the $NaPF_6$-based diglyme electrolyte, the performance of AFSMBs can be efficiently improved.[37] As a matter of fact, uniform Na nucleation and deposition on the modified Al current collector has been achieved in this bi-salt electrolyte system (Fig. 7a), contributing to the B-containing SEI and CEI derived from the decomposition of $NaBF_4$. Consistent with theoretical calculations, both PF_6^- and BF_4^- can infiltrate the first solvation sheath of Na^+, and the LUMO and HOMO energy levels of $NaBF_4$ are both higher than the $NaPF_6$-dominated one (as shown in Fig. 7b), suggesting that the formation of unique interfacial chemistry with the preferential reduction of $NaBF_4$ to form SEI or CEI compared to $NaPF_6$. As depicted in Fig. 7c, the presence of $NaBF_4$-derived interphases enabled the dense and dendrite-free Na deposition morphology. Leveraging the synergistic effects of the $NaPF_6$–$NaBF_4$ dual-salt electrolytes, the AFSMBs coupled with high-voltage layered oxide cathode exhibit an extended cycle life up to 260 cycles without the imposition of external pressure. Furthermore, these batteries, prioritized for safety at the A h-scale, offer an exceptional energy density over 200 W h kg^{-1} (Fig. 7d).

Sodium trifluoromethanesulfonate (NaOTf), another important sodium salts with a large anion, has also been reported.[115,116]

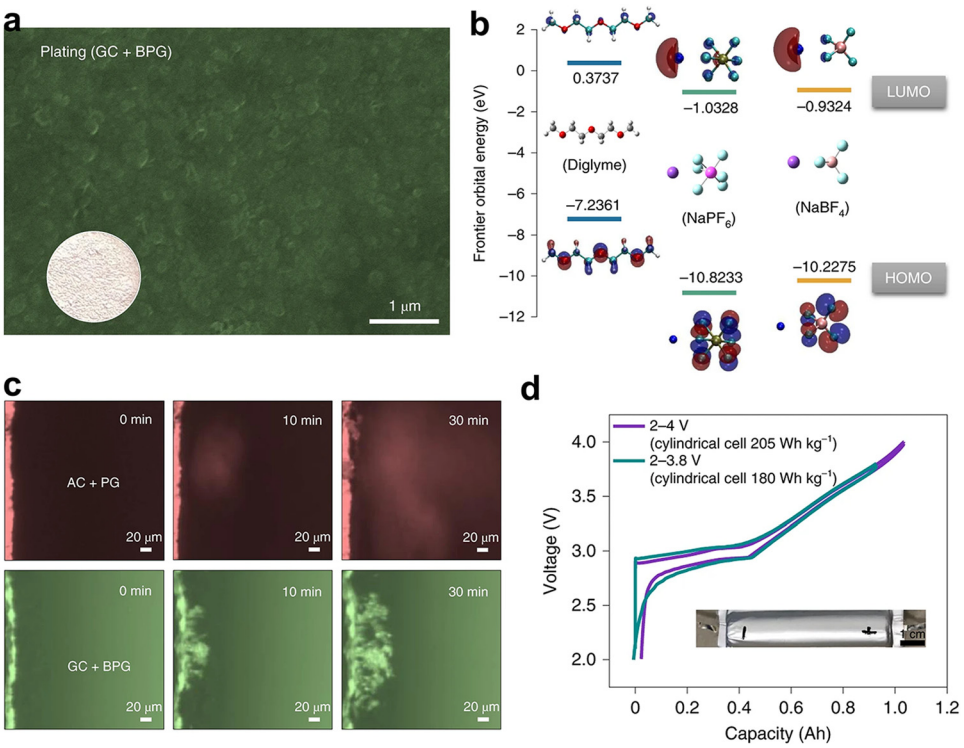

Fig. 7 (a) SEM image of Na deposition in the AFSMBs using GC and BPG after ten cycles. The inset shows the related digital image. (b) Molecular orbital energies of diglyme, $NaPF_6$, and $NaBF_4$, including LUMO and HOMO energies. (c) *In situ* optical microscopic observation of Na plating in the AFSMBs using AC plus PG (a) and GC plus BPG. (d) Galvanostatic third discharge/charge curves of the AFSMBs (cylindrical cell) using GC plus BPG with different cut-off voltages at a current rate of 0.5 A. The inset shows the image of an 1 A h level anode-free cylindrical cell with an energy density >200 W h kg^{-1}. Reproduced with permission.[37] Copyright 2022 Nature Publishing Group.

Its combination with linear ether solvents demonstrated a promising way to realize low-temperature electrolytes, where the OTf^- anion is found to form a stable SEI at low temperatures. For example, Thenuwara *et al.* developed a dual-salt electrolyte consisting of 0.8 M NaOTf and 0.2 M $NaBF_4$ dissolved in diglyme.[117] The synergy between NaOTf and $NaBF_4$ salts promotes the uniform and compact morphology of the sodium deposits at low temperature, as well as high ionic conductivity and robust SEI formation with high inorganic content on stainless steel substrate, stabilizing the Na-metal plating/stripping process. Due to the altered decomposition kinetics of salts, the dual-salt electrolyte induced inorganic-rich SEI formation occurs at both 20 and −40 °C, but the SEI formed at the lowest temperature was much thinner, resulting in lower charge transfer resistance. In addition, the atomic concentrations of various elements in SEI confirmed lower organic species amount, which is chemically distinct from that one under 20 °C (Fig. 8a). These results suggest that the development of low-temperature AFSMBs with high stability is possible by designing dual-salt ether-based electrolytes to control sodium deposition and SEI composition.

A weakly solvated dual-salt diglyme (G2) electrolyte containing 0.6 M NaOTf and 0.4 M $NaBF_4$ was investigated in low-temperature AFSMBs.[118] An ultrahigh average CE of 99.88%

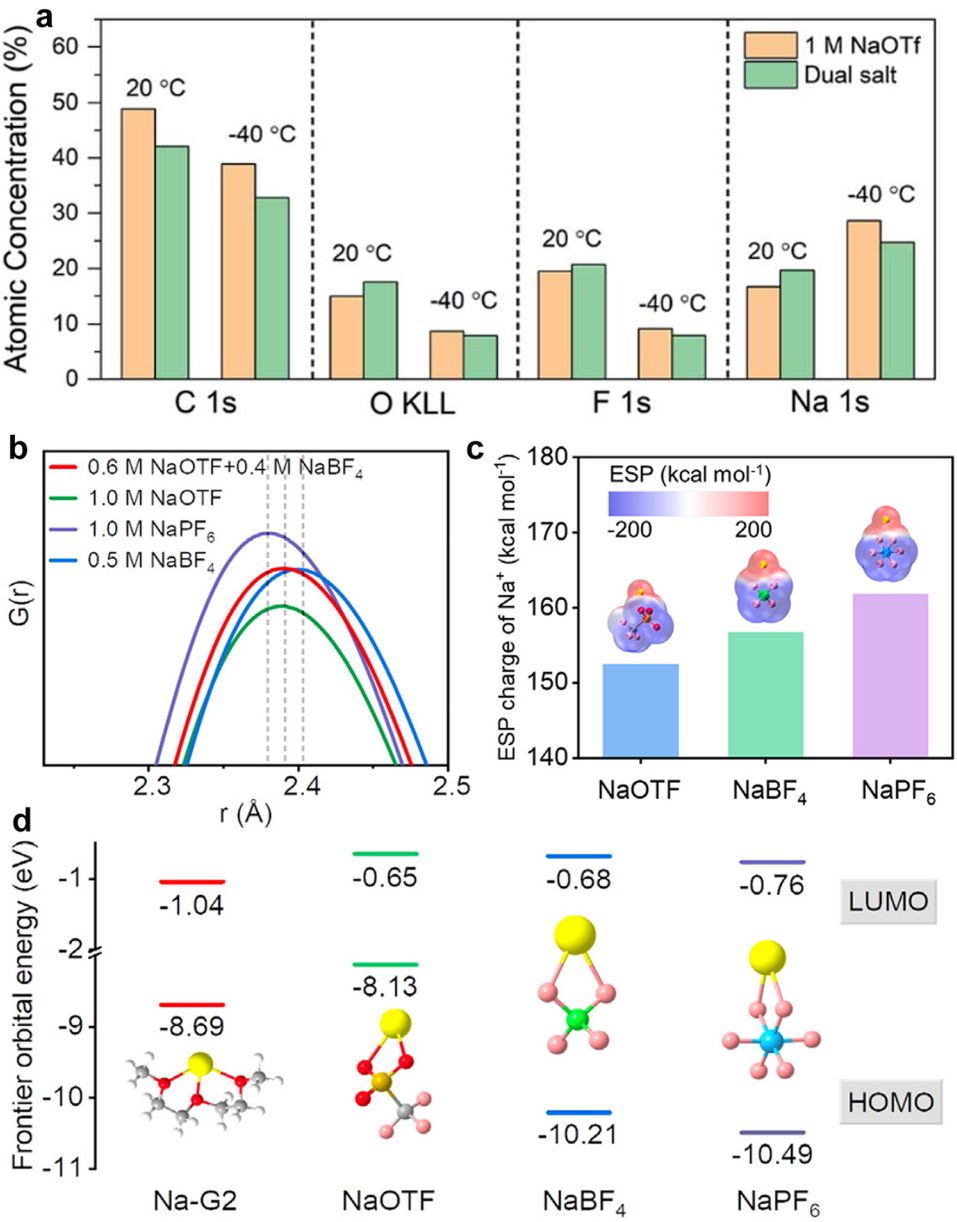

Fig. 8 (a) Atomic concentrations of various species measured by integrating core level spectra of SEI samples generated at different temperature. Reproduced with permission.[117] Copyright 2021 The Royal Society of Chemistry. (b) RDF of Na^+–O(G2) obtained from theoretical calculations for different electrolytes. (c) ESP mapping of different Na^+–anion complexes. (d) LUMO and HOMO energy levels of Na–G2, NaOTF, $NaBF_4$, and $NaPF_6$. Reproduced with permission.[118] Copyright 2024 Elsevier.

was achieved at −40 °C on Al current collector, indicating good compatibility and reversibility with anode due to the formation of a B/F inorganic-containing SEI. In addition to the SEI, the solvation behavior of Na^+ ions plays a significant effect on low-temperature performance of batteries. According to the radial distribution function results, the Na–O (G2) distance, reflecting the interaction between Na^+ ions and solvent molecules, increases when the anion changed from PF_6^- to OTF^- and BF_4^- (Fig. 8b), and the coordination number of Na with O (G2) was also reduced from 5.85 to 5.38. Meanwhile, the lower electrostatic potential (ESP) charge compared to Na^+ in $NaPF_6$ is displayed due to the stronger electron-donor effect of OTf and BF_4, leading to longer bond lengths between Na^+ and O (G2) with weak solvation effect (Fig. 8c), which enables a faster desolvation process.[119] In addition, $NaBF_4$, with a higher LUMO level, tends to decompose prior to NaOTf at the anode side, contributing to F/B inorganic-rich SEI formation (Fig. 8d), while it remains stable at the cathode side due to its low HOMO level, which ensures the stable operation of high-voltage cathode.

In the realm of either co-solvent or dual-salt strategies to modulate the electrolytes, the main challenges stem from unstable solvation structures and electrolyte decomposition that can be triggered by one of the components, resulting in the unstable SEI formation. The introduction of different solvents and salts can alter the solvation structure, which in turn affects the desolvation process. To tackle these issues, high-concentration electrolytes can be employed to provide a wide electrochemical stability window and suppress dendrite growth. Additionally, combining strong and weak solvating solvents may creates a hierarchical solvation structure that optimizes the electrolyte's properties. The selection and combination of different salts or solvents is also challenging, to ensure that each can exert its own advantages without sacrificing the unique properties of the electrolyte. This requires careful selection and optimization of the combinations to achieve a balanced and effective electrolyte system.

3.5. Solid-state electrolyte

Although conventional liquid electrolytes are designed to regulate Na deposition behavior and interfacial chemistry, several challenges still need to be overcome when using in practical applications. The major bottleneck is that the liquid electrolytes inevitably react with the active (SEI uncoated) sodium metal and continuously generate the porous or mossy-like passivation layer, resulting in a constant depletion of sodium inventory.[20] However, the adoption of solid state electrolytes (SSE) in AFSMBs can significantly reduce the interfacial reactions of electrolyte/current collector because of the contact between SSE and current collector shifts from three-dimensional to planar. Additionally, a denser sodium metal deposition can be formed on the current collector, enabling the main advantage of reducing approximately 15% cell stack volume, thus contributing to an increased volumetric energy density (Fig. 9a and b). Therefore, anode-free solid-state sodium metal battery (AFSSB) concepts are explored to promise a safe and high energy density battery technology with less material consumption and simple anode processing. However, the homogeneous and uniform electrochemical deposition of alkali metal at the interface between current collector and SSE plays the central role in the successful operation of AFSSB configuration.[120] For example, in an anode-free solid-state lithium cell configuration, the uniform deposition of lithium metal in a capacity of 5 mA h cm^{-2} requires around 24 μm thickness,[121] while it would increase to ~44 μm in the case of sodium on account of higher molar volume of sodium metal, showcasing the importance of the interfacial adhesion on the nucleation and growth behavior.[122]

Recently, the sodium deposition behavior on the interface between Cu and NASICON-type SSE ($Na_{3.4}Zr_2Si_{2.4}P_{0.6}O_{12}$, NZSP) was investigated at different current densities and stack pressures (Fig. 9c and d).[122] It was found that both the current density and stacked pressure would affect the nucleation and deposition behaviors of Na at the Cu|NZSP solid–solid interface. At higher current density, the optical 3D confocal microscopy images revealed inhomogeneous sodium growth on the Cu electrode. In contrast to stack pressure, a higher degree coverage on the electrode was displayed with the increase of current density, which demonstrates the higher current density contributing to more uniform sodium deposition (Fig. 9e). This result is opposite to the cognition that higher pressure would induce an inorganic-rich SEI with more uniform and denser Li film in metallic Li system.[124] These results evidence that the deposition of sodium at the interface between Cu current collector and SSE can be achieved, while the feasibility on anode-free sodium-based full cell is still scarce.

Except from the current density and stack pressure manipulations at the interface, the types of current collectors, which can alleviate the internal strain, lower the local current density,[30,125] and prolong the cycle life, also affect the deposition behaviors. Even though the surface modification of current collectors can control the electrodeposition morphology to be more reversible and homogeneous, improving the contact between the SSE and current collector is very critical for repeated sodium plating/stripping. Recently, a stable sodium borohydride SSE has been identified to form near-perfect contact with a pelletized Al current collector through cold pressing.[123] Such a dense interface can effectively prevent the infiltration of sodium dendrites and enable sodium stripping/plating at a high current density up to 6 mA cm^{-2}. Further demonstrating the feasibility, an anode-free sodium all-solid-state battery featuring $NaCrO_2$ as the cathode was tested under a stack pressure of 10 MPa and at a temperature of 40 °C, exhibiting a remarkable average CE of 99.96% over 400 cycles. This work delineates the pivotal direction of designing advanced electrolyte to optimize the solid–solid interface in AFSSBs that governs the electrochemical performance.

To date, the application of AFSSBs is still limited in NASICON-type and sodium borohydride SSEs. Other types of SSEs yet to be explored include sulfide-based electrolytes, polymer electrolyte or hybrid ones, and focus should be paid on understanding the performance of the existing electrolyte systems by examining the properties and interactions of these

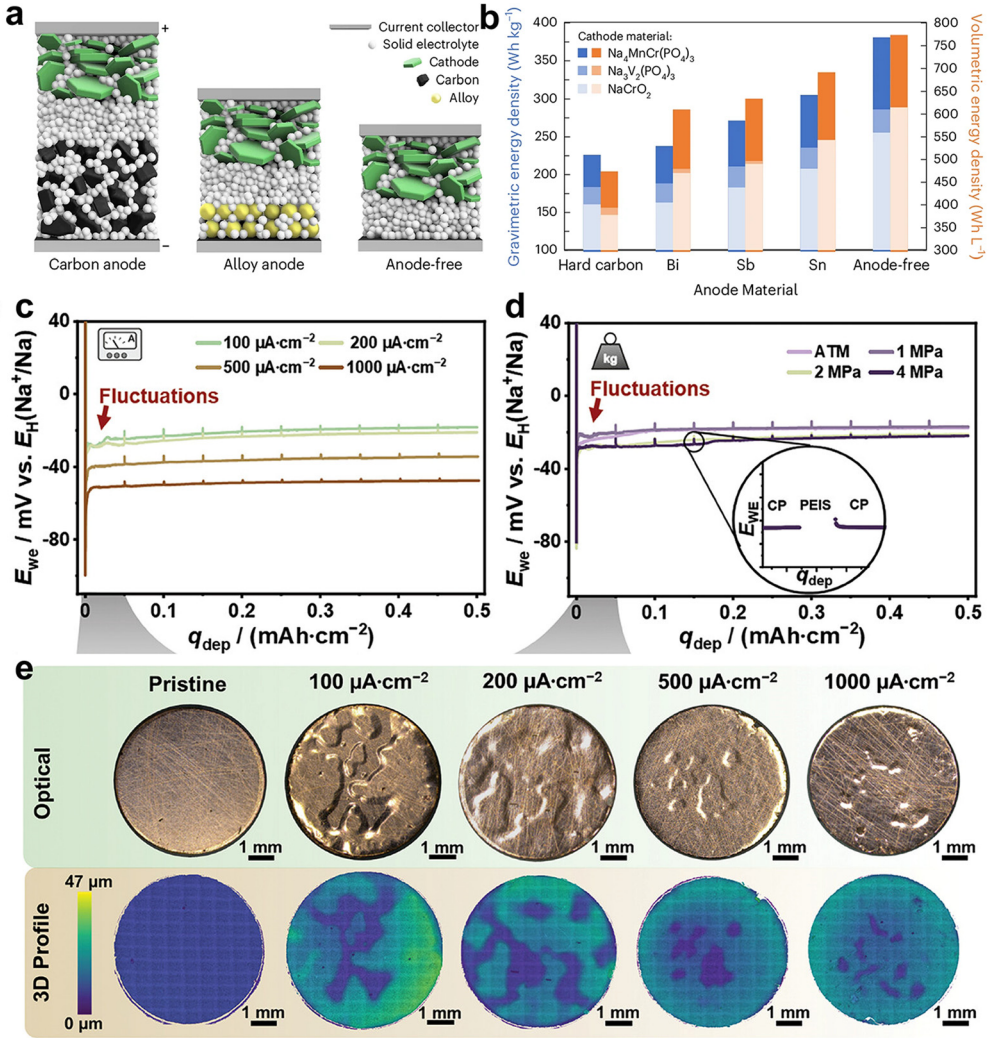

Fig. 9 (a) Cell schematic for carbon anodes, alloy anodes and an anode-free configuration, showing the advantage to design anode free solid state sodium batteries. (b) Theoretical energy density comparison for various sodium anode materials. Reproduced with permission.[123] Copyright 2024 Wiley-VCH GmbH. (c) and (d) Potential profile of cathodic deposition of sodium at Cu|NZSP interface at various current densities and stack pressures. (e) Optical microscopy images of the copper electrode pristine after cathodic deposition with q_{dep} = 0.5 mA h cm^{-2} at various current densities (upper row) and corresponding 3D profiles (lower row). Reproduced with permission.[122] Copyright 2023 Wiley-VCH GmbH.

alternative solid electrolytes within an anode-free configuration. To design a practical AFSSB, the electrolyte selection and their compatibility with current collector will be the key factors in determining the cell performance, raising the following specific considerations: (i) high electrochemical stability of SE to construct a stable electrode/electrolyte interphase, reducing the consumption of sodium inventory; (ii) stable interface contact between current collector/SE to guarantee high reversible plating/stripping on the current collector; (iii) highly dense solid electrolyte to suppress sodium dendrites; (iv) highly inert current collector to reduce interfacial side reactions. Furthermore, it needs to be emphasized that a high loading cathode and thin SSE ($\leq$20 μm) would be also required to enable a practical cell architecture to guarantee the advantage of high energy density of AFSSB, which will bring more critical mechanical requirements for SSE.

4. Interphase optimization for modulating interfacial ion/atom diffusion

4.1. Electrolyte-derived SEI

In the AFSMB configuration, the sodium metal anode is not pre-deposited, but forms as the battery is charged for the first time. Accurately understanding the formation mechanism of SEI layer on anode is always crucial, but unique for AFSMB investigations because it grows on the inert electrode.[126]

In SMBs, the growth of the SEI layer in liquid electrolytes is expected to occur from bottom to top through three main stages (Fig. 10a) leading to the formation of inorganic-based inner SEI components and generating the mosaic structure.[63,127,128] In this process, the SEI thickness continuously grows due to the

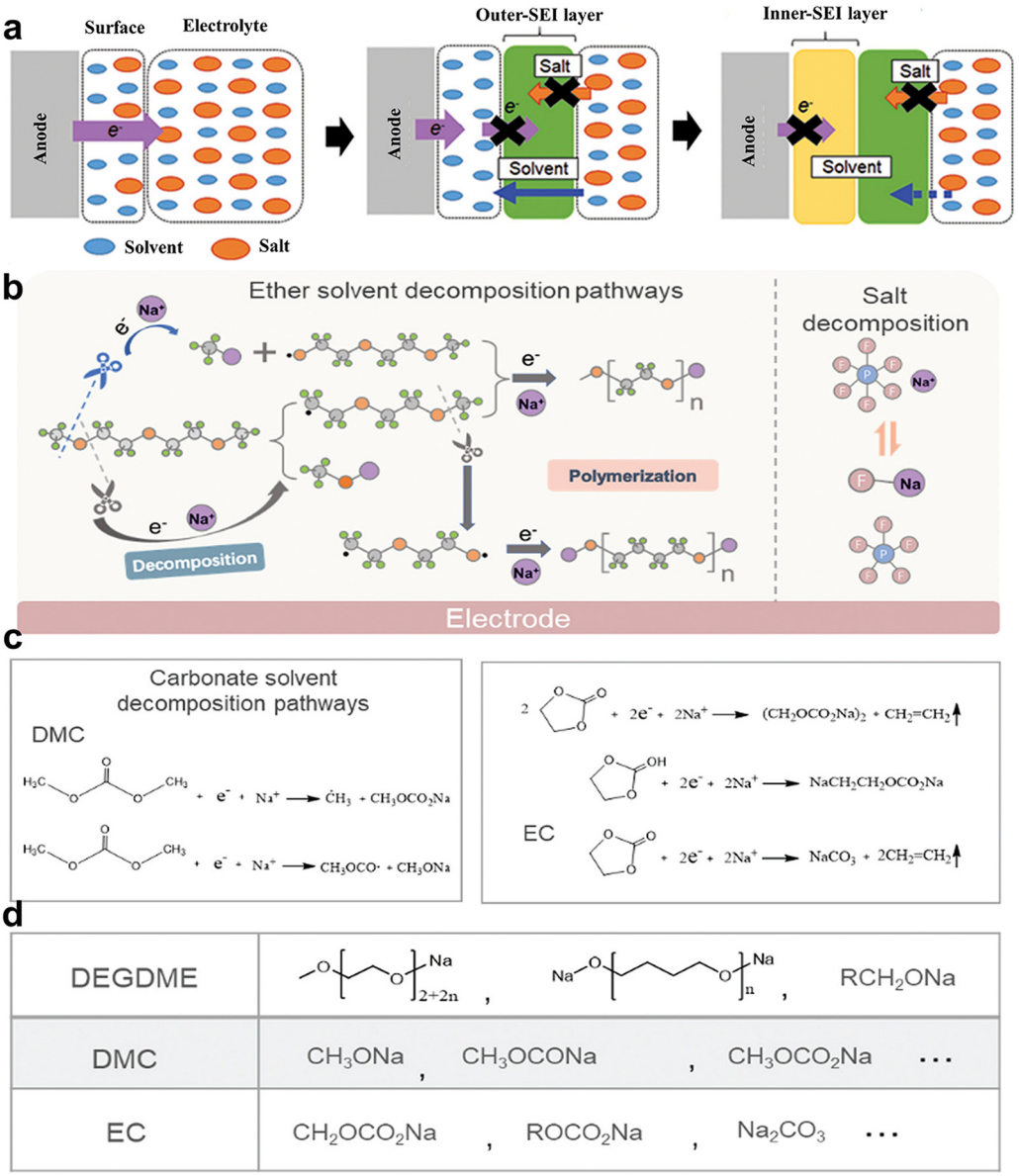

Fig. 10 (a) Diagram illustrating the "bottom-up growth mechanism" of SEI layer in the electrolyte as interpreted by the red moon simulation. Reproduced with permission.[127] Copyright 2021, Wiley-VCH. Schematic representation depicting the decomposition pathways of (b) ether solvent (DEGDME) and (c) carbonate solvents (DMC and EC). (d) Overview of the decomposition products of DEGDME, DEC, and EC. Reproduced with permission.[128] Copyright 2022, The Royal Society of Chemistry.

stepwise decomposition of the electrolyte's components until the entire electrode surface is fully covered, effectively inhibiting further reduction of electrolytes in contact with electron from the electrode. In AFSMBs, the substantial differences in the chemical and electrochemical reactivities of substrates for sodium deposition can lead to varying SEI components and homogeneity, which are also crucial factors in enhancing cell performance.[129]

Based on the proposed SEI formation mechanism, the chemical composition of the SEI is predominantly determined by the components in the electrolyte, *i.e.*, sodium salts, solvents, and additives.[79,128,130] Typically, the typical SEI consists of a mixture of inorganic and organic species, which are mainly sodium species, including Na–O, Na–F, Na–CO_3, Na–PO_4, Na–PFO, Na–S_x, Na–SO_x, Na–N_x, and Na–NO_x, depending on the type of solvents and salts in the electrolytes. Despite their poor anti-oxidation property, glymes (mono-, di-, and tetraglyme)-based electrolytes offers the highes CEs for sodium stripping/plating reactions on inert current collectors, making them suitable for AFSMBs. In the context of ether-based electrolytes for sodium batteries, the discharge process involves electron transfer that targets electrophilic centers, such as carbon atoms in the ether, leading to bond cleavage (Fig. 10b) further enhanced by BF_3^- and/or PF_5^- derived from the partial decomposition of $NaBF_4$ or $NaPF_6$.[131] The cleavage process leads to the formation of radical species and organic sodium alkoxides

(RCH_2ONa), which further induces the polymerization of polymer-like species owing to the radical generation.[132] The $NaPF_6$-based electrolytes in sodium batteries outperform those based on $NaClO_4$- and NaTFSI-based electrolytes, due to the catalytic formation of inorganic species from salts and the presence of polymer-like species in the SEI.[133,134] These factors, as practically proven, contribute to the improved electrochemical performance through the ether-based electrolyte optimization strategies mentioned earlier for AFSMBs. Besides, tremendous efforts have been devoted to improving Na metal stability by modulating the NaF-formation in the SEI layers by addtivie strategies.[79,135] For example, perfluorobenzene as an additive has been used to construct robust NaF-rich SEI that inhibits dendrite growth and enables stable sodium anode operation.[136]

Although carbonate-based electrolytes exhibit greater oxidation stability, their poor compatibility with sodium metal anodes renders them unsuitable for sodium metal batteries.[137,138] For comparison, the decomposition pathways and resultant products of conventional carbonate-based electrolytes (EC and DMC) are illustrated in Fig. 10c and d, respectively. Conventional carbonate-based electrolytes like EC and DMC primarily produce organic $ROCO_2Na$ and inorganic Na_2CO_3 upon decomposition, inducing unstable SEI layers. In contract, the higher LUMO values of ether-based solvent–cation complexes indicate greater stability against reduction, leading to less decomposition and thinner SEI layers and consequently contributing to high initial CE (ICE) and fast ion transport by shortening the diffusion length.

4.2. Artificial interphase layers on current collectors

The electrolyte-induced interface chemistry by electrolyte optimization strategies is efficient yet complicated in an anode-free cell. Besides, the design of an artificial interphase layer on the current collector is showing promise to guide nucleation, prevent dendrite growth, and ensure uniform deposition of sodium metal.[139] Effective artificial design in AFSMBs primarily focused on two distinct considerations: the introduction of a nucleation layer and the construction of an artificial SEI as a buffer layer. Within the context of nucleation layer modification, the fundamental principle relies on the fact that the sodium plating on the current collector is predominantly governed by the sodiophilic nucleation sites with a high affinity to Na^+, which must overcome a certain nucleation barrier for deposition. Therefore, the modulation of nucleation sites by an artificial layer can optimize sodium deposition behaviors to achieve higher CE and homogenous deposition morphology.[140–142]

Carbon materials are promising candidates for the design of nucleation layers in sodium deposition, due to their similar potential and compatibility with most electrolytes. For example, a nanocarbon layer directly casted onto Al foil (Fig. 11a) showed a lower nucleation energy barrier compared to the bare Al (Fig. 11b), thereby facilitating the Na nucleation and resulting in a stable plating behavior.[38] As a result, high average CE (99.8%) and low voltage hysteresis were achieved during long-term plating/stripping cycles. Furthermore, Cohn *et al.* conducted an in-depth investigation into the efficacy of insertion-type (non-graphitized carbon, *i.e.*, carbon black and hard carbon) and alloy-type (bismuth, Bi) materials as nucleation layers to regulate the initial sodium plating process in an anode-free configuration (Fig. 11c and d).[143] The results revealed that the energetics of sodium nucleation and the resulting CE are dependent on the nucleation layer composition, in which the carbon black nucleation layer enables higher sodium plating–stripping CEs than hard carbon. Based on these findings, anode-free cells coupled with $Na_3V_2(PO_4)_3$ cathodes were fabricated, reaching energy density up to 318 W h kg^{-1} at 0.25 mA cm^{-2} (Fig. 11e) and a capacity retention of 82.5% after 100 cycles at 0.5 mA cm^{-2} (Fig. 11f). These results underscore the pivotal role of nucleation layer composition in enhancing the electrochemical performance of AFSMBs.

Since the nature of carbon affects the sodium nucleation behavior, accordingly amorphous and graphitic carbon coatings on Al foils were investigated.[37] The highly graphitized carbon showed higher electronic conductivity and possessed more intricate pore network, which enhances the electrolyte wettability with respect to amorphous carbon (Fig. 12a and c). This obvious difference in material properties resulted in the irregular sodium lumps with cracking, while more uniform and smaller sodium metal blocks were present on graphitized carbon, gradually forming a dense deposition layer on the substrate. Such different morphology further influenced the durability of SEI upon plating/stripping cycle. On graphitized carbon, a thinner SEI layer was observed with less dead sodium, contrasting with the amorphous carbon of possessing a thick SEI layer and substantial dead sodium coverage (Fig. 12b and d).

As previously reported, the presence of defect-rich pyrrolic and pyridinic N sites in a carbon framework can disrupt the π-orbital resonance and electron density distribution, leading to an electron-deficient state to bind Na.[144] As shown in Fig. 12e, the plasma-treated carbon-coated Al anode current collector was prepared to introduce pyrrolic and pyridinic N-doped sites on the surface (p-Al@C).[118] Density functional theory (DFT) calculations (Fig. 12f and g) indicate that the introduction of N-doped sites significantly enhanced sodium adsorption energy. Specifically, the interactions of Na atom with graphitic N (−0.28 eV), pyrrolic N (−1.67 eV), and pyridinic N (−1.33 eV) were substantially stronger than that with the pristine carbon site (−0.18 eV), indicating the well-improved sodiophilicity of the N-doped carbon layer. Moreover, the compositions and structure of the electrolyte-derived SEI would also be affected in the presence of the N-doped carbon layer. As depicted in Fig. 12h, the surface of p-Al@C exhibited an increase in inorganic components, such as NaF, Na_2O, and B_2O_3, with extended etching duration when cycled in an optimized ether-based electrolyte, implying a progressive enrichment of inorganic species from the outer surface towards the inner layers of the SEI.[145]

Apart from the representative carbon nucleation layers, other metallic alloy materials such as the Bi[139] and Zn,[146] can also effectively influence the sodium deposition process and exhibit high affinity for sodium. For example, the Cu@Bi layer was designed through a facile *in situ* reduction reaction, in which the Bi nanoparticles can be transformed into a sodiophilic, sodium-rich alloy phase, thereby enhancing the

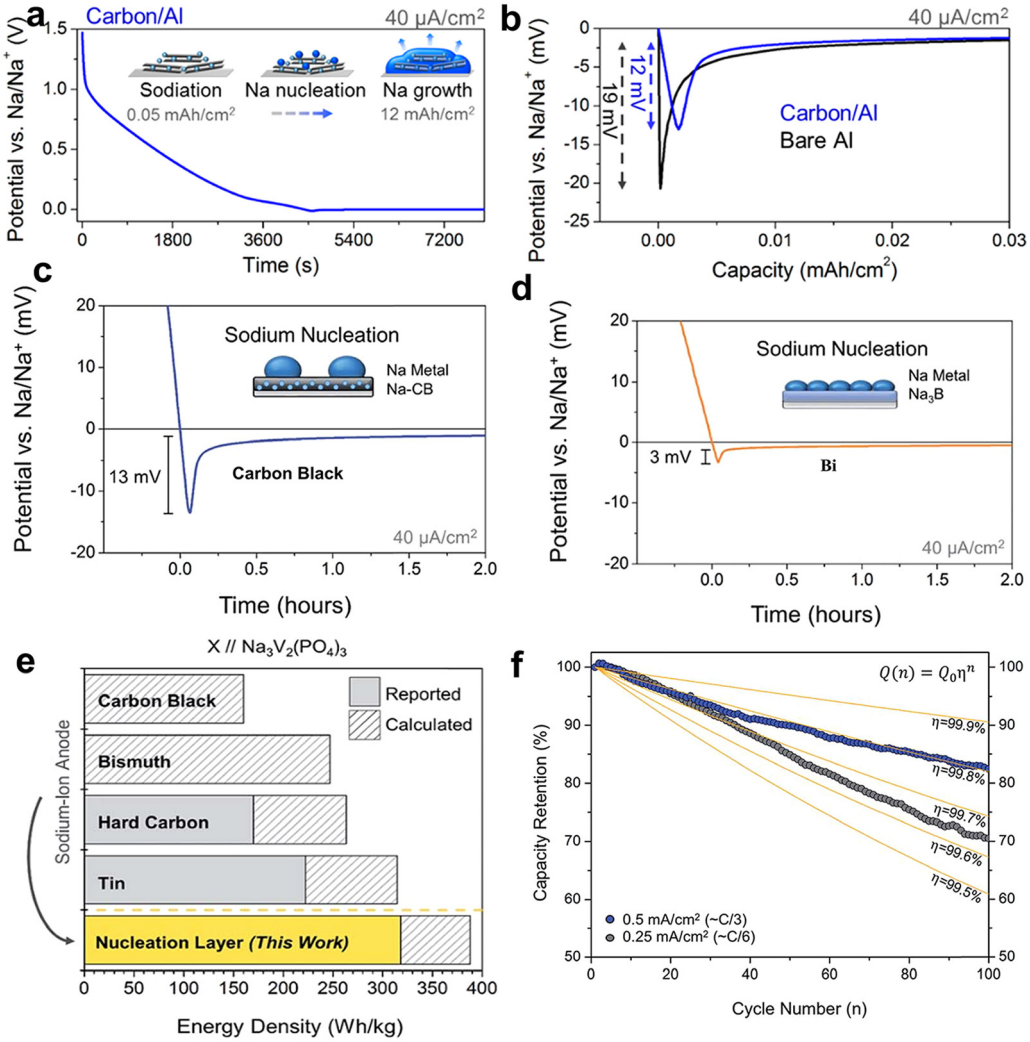

Fig. 11 (a) Galvanostatic sodiation and plating process for carbon/Al current collector at 40 μA cm^{-2}. (b) Comparison of the sodium nucleation overpotential for bare Al and carbon/Al current collectors at 40 μA cm^{-2}. Reproduced with permission.[38] Copyright 2017 American Chemical Society. (c) Na metal nucleation profiles at 40 μA cm^{-2} on sodiated electrodes using carbon black and Bi as nucleation layer. (e) Energy density comparison among battery configurations employing distinct anode paired with a $Na_3V_2(PO_4)_3$ cathode. (f) Cycling capacity retention with decay curves plotted for anode-free cells at 0.5 mA cm^{-2}. Reproduced with permission.[143] Copyright 2018 The Royal Society of Chemistry.

formation of a homogenous and dense sodium metal layer upon plating. Although the construction of artificial interphases using conventional carbon hosting and metal seeding layers known for their high sodium affinity is beneficial, the increased side reactions at the large electroactive surface and the initial sodiation reaction with alloying steps will inevitably cause high sodium ion consumption. Thus, how to design an outstanding sodiophilic layer that regulates sodium deposition with minimal sodium ion consumption is a tough challenge. Interestingly, an elaborately-designed porous triazine framework with integrated fluorine functionality as hosting/seeding interphases on Al current collector results in delivering excellent sodiophilicity yet low Na ion consumption.[48] This well-defined layered framework with fluorinated groups offers highly-ordered porous channels for sodium ion flux and nucleation sites, resulting in homogeneous sodium deposition and reduced sodium reactivity for Na ion depletion. More recently, a thin high-entropy alloy nanolayer composed of Nb, Mo, Ta, W and V nanoplates on Al foil, has been showed to own high sodiophilicity, thus reducing the overpotential for Na deposition.[147] Consequently, dendrite-free Na deposition, low nucleation and remarkable CEs were achieved, propelling the practical implementation in anode-free Al‖$Na_3V_2(PO_4)_3$ batteries.

These results clearly demonstrated the efficient construction of artificial interphase layers that can improve their Na affinity (sodiophilic properties) and facilitate SEI formation. The introduction of porous carbon hosting layer can also significantly buffer the internal strain caused by the initial Na metal deposition, providing sufficient nucleation sites. Our previous work also reported a robust and porous sodiophilic layer by applying MOF-derived Cu@carbon composites to conventional current collectors (both Al and Cu), providing abundant nucleation sites to guide Na deposition and inhibiting the sucessive dendrite growth (Fig. 13a).[47] The galvanostatic plating results

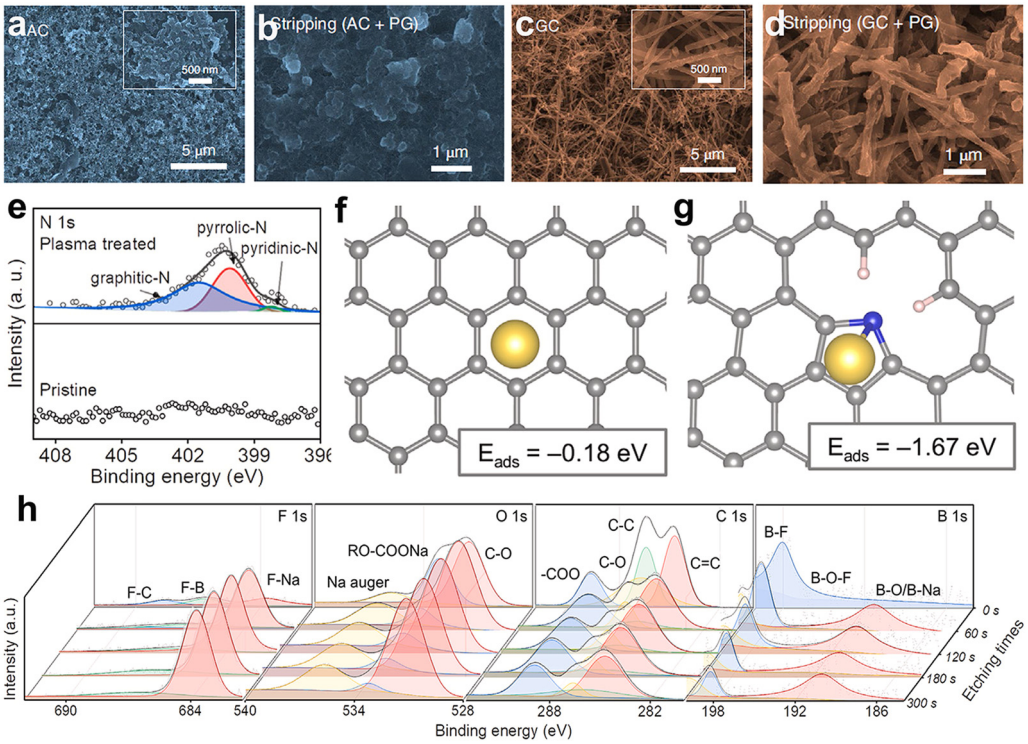

Fig. 12 SEM images of (a) and (b) amorphous carbon and (c) and (d) graphitized carbon before and after Na stripping in the AFSMB. Reproduced with permission.[37] Copyright 2022 Nature Publishing Group. (e) N 1s XPS spectra of different current collector, including pristine Al@C and p-Al@C. Relaxed configurations of Na atom absorbed on various substrates: (f) perfect carbon and (g) N-doped carbon (inset is adsorption energy E_{abs}). (h) XPS analysis of the SEI formed on deposited Na using p-Al@C current collector with different sputtering time. Reproduced with permission.[118] Copyright 2024 Elsevier.

demonstrate that the incorporation of Cu@C composites substantially decreased the nucleation barrier for Na plating on both Cu and Al current collectors, indicating for enhanced sodiophilic properties (Fig. 13b). Moreover, *in situ* electrochemical dilatometry results revealed that the as-prepared Cu@C layer plays a crucial role in the early stages of sodium plating facilitating the formation of an efficient SEI during the initial sodiation process. This SEI effectively curtails side reactions, such as continuous electrolyte consumption and accumulation of inactive Na, consequently promoting more uniform and denser Na deposition without significant volume changes in contrast to a bare Cu foil (Fig. 13c).

Besides these efforts, it is still challenging to fabricate ideal artificial interphase layer by introducing additional materials. For example, the widely adopted carbon-based materials cannot avoid the side reactions at initial cycles, leading to notable sodium ion depletion and electrolyte consumption. The porous structure, either inheriting from the bulk materials structure or resulting from the fabrication process such as wet-casting with a thickness in micrometers, will reduce the overall volumetric energy density at A h-level. Therefore, it is essential to balance the benefits of the artificial interphase technology with battery performance parameters, especially the gravimetric and volumetric energy densities. Accordingly, developing novel fabrication approaches involving a combination of efficient materials can precisely manipulate the interfacial layers on the substrate.

Recently, a novel strategy for fabricating an Al current collector through annealing and direct fluorination using hydrofluoric acid, as schematically presented in Fig. 14a, has been reported.[148] Such annealing treatment induced the highly preferential orientation along the (100) crystal plane. By further fluorination, the Al substrate (F-A-Al) exhibited much lower binding energy with Na (Fig. 14b and c), providing more nucleation sites and enabling planar deposition of Na as illustrated in Fig. 14d. This surface modification enhanced the Na nucleation/growth process and facilitated the reversibility of Na deposition/dissolution process (Fig. 14e and f). Coupling with an ionic liquid electrolyte, the demonstrated AFSMB employed with $Na_3V_2(PO_4)_3$ cathode delivered higher energy density and CE. These findings indicate promising potential for interfacial modification of current collectors with enhanced sodiophilicity, facilitating the performance of anode-free batteries with enhanced efficiency and extended operational lifespan. Eventhough, artificial interphase layers in AFSMBs still confront challenges like poor mechanical stability, limited sodiophilicity, insufficient ionic conductivity, and weak adhesion to current collectors. These issues can lead to heightened interfacial resistance and dendrite formation. Moreover, the fabrication processes are often intricate and multi-step, posing difficulties for large-scale applications. To enhance electrode compatibility, strategies such as employing multicomponent interphase layers to boost mechanical strength and sodiophilicity, developing advanced fabrication techniques for improved surface adhesion, and optimizing interphase layer composition with materials of high ionic conductivity can be adopted.

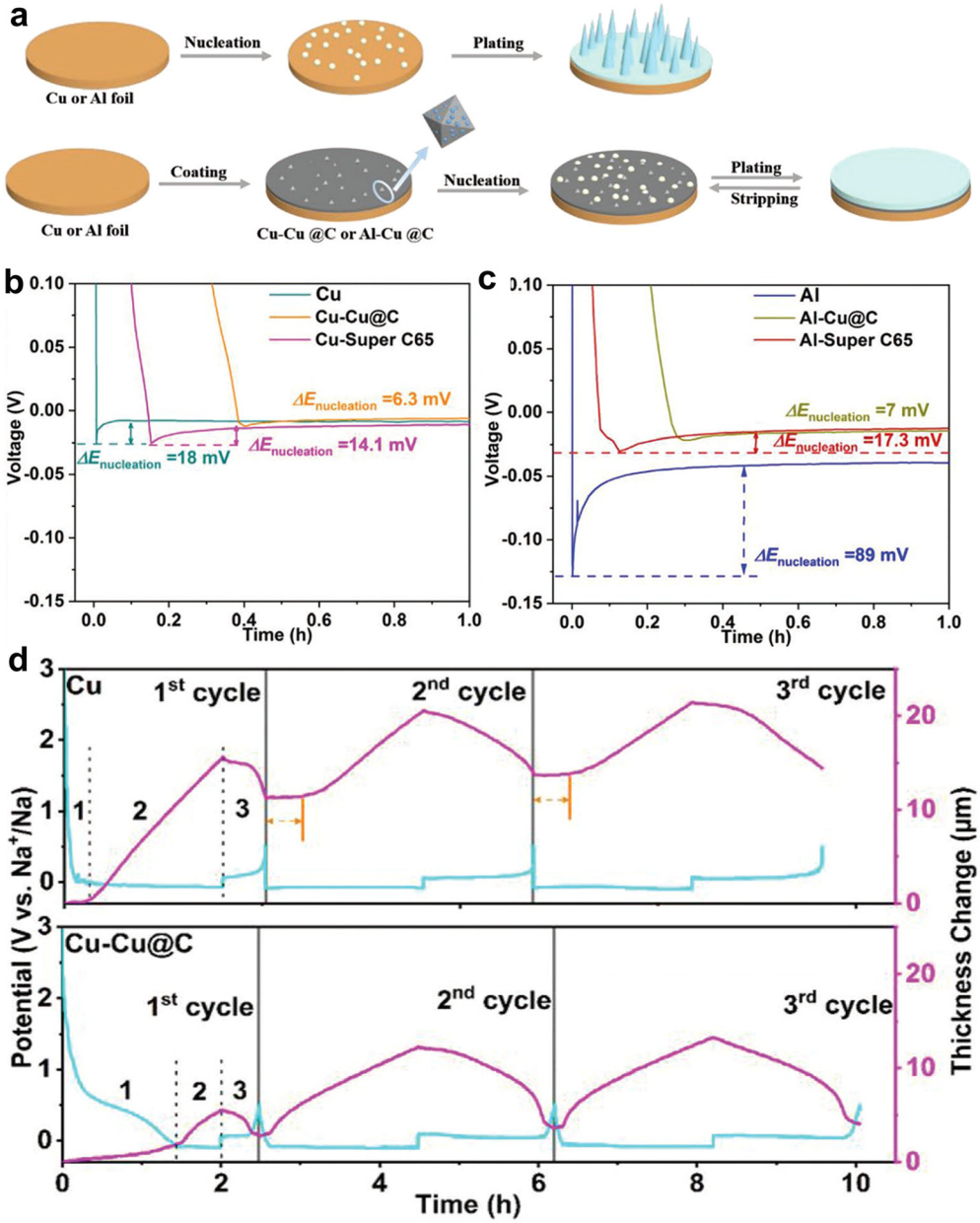

Fig. 13 (a) Schematics of Na deposition on bare Cu or Al foils and Cu–carbon composites coated current collectors. (b) and (c) Comparison of the sodium nucleation overpotential in different cells. (d) *In situ* dilatometry investigation of bare Cu and Cu–Cu@C electrodes at a current density of 0.5 mA cm^{-2}, with a fixed Na plating charge of 1 mA h cm^{-2}. Reproduced with permission.[47] Copyright 2022 Wiley-VCH GmbH.

4.3. Architecture designs of current collectors

An alternative strategy to enhance the cycling stability of AFSMBs involves the promotion of uniform sodium metal deposition by manipulating the physicochemical properties and surface microstructures of the anode current collectors. This approach diverges from the previous ones, which focused on the application of an artificial layer to refine the deposition behavior of sodium on conventional current collectors. Here the emphasis is placed on the material and architecture of current collectors. These factors are critical as they substantially affect the nucleation of sodium and the subsequent formation of the SEI, which in turn influence the overall electrochemical performance of battery. To effectively control sodium plating and stripping in AFSMBs, the ideal anodic current collector substrate should satisfy the following criteria: (i) exceptional mechanical strength to withstand the internal pressure changes that occur with the rapid volume fluctuations associated with sodium deposition; (ii) high electron conductivity is necessary to maintain a surface potential equilibrium, facilitating the uniform Na deposition; (iii) low surface diffusion energy for sodium ions and atoms, aiding the lateral diffusion of sodium and ensuring even distribution to nucleation sites; (iv) high surface affinity for sodium to create a thermodynamically favorable state that promotes a dendrite-free sodium deposition morphology; (v) robust

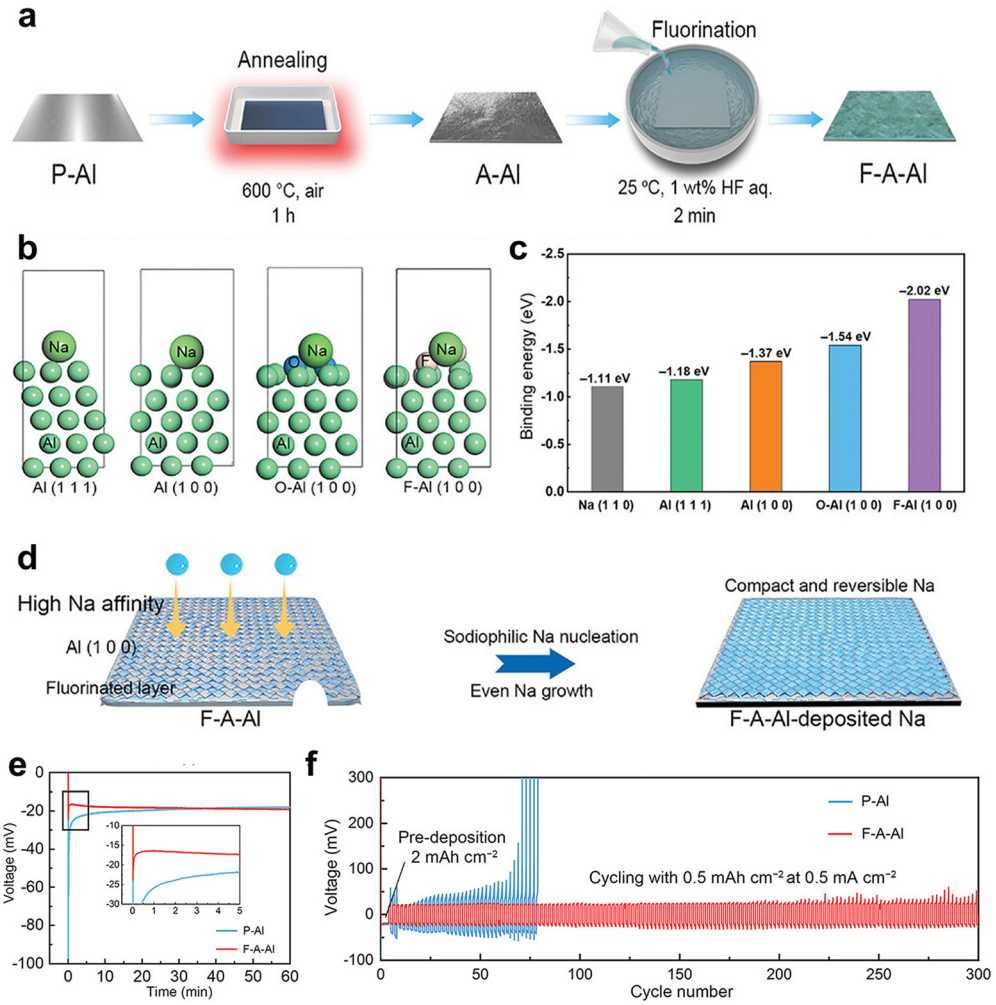

Fig. 14 (a) Schematic illustration of the fabrication process of the annealed Al (A-Al) and fluorinated annealed Al (F-A-Al). (b) Adsorption model of Na atom on Al (111), Al (100), oxidized Al (O-Al (100))and fluorinated Al surface (F-Al (100)) for DFT calculations. (c) Binding energies of Na atom on different substrates based on the DFT calculations. (d) Schematic illustration of the interfacial behavior during Na deposition on different Al current collectors. (e) Comparison of the voltage profiles of the Al/Na cells for P-Al and F-A-Al substrates during the galvanostatic Na deposition at 0.5 mA cm^{-2} for 0.5 mA h cm^{-2}. (f) Voltage profiles of the Al/Na cells for P-Al and F-A-Al during Na metal deposition/dissolution tests with pre-deposited Na metal (2 mA h cm^{-2}). Reproduced with permission.[148] Copyright 2023 Wiley-VCH GmbH.

electrochemical stability to prevent corrosion and mitigate side reactions at the electrolyte/electrode interface.

The use of anodic current collectors with specific micro- and/or nanostructures, known as 3D electrode hosts, is beneficial for achieving uniform Na deposition and prolonging the lifespan of AFSMBs.[149] Specifically, these 3D porous structured current collectors can facilitate a controllable nucleation and growth process for Na metal deposition.[150] On one hand, the 3D-structured hosts provide sufficient a buffer to alleviate the volume change associated with Na metal plating/stripping, thus mitigating the mechanical stress that can lead to dendrite formation and capacity loss.[47] On the other hand, the 3D porous architecture is adept at managing ion flow and offering large surface area with nucleation sites. This design reduces the local current density, which is crucial for preventing high currents at specific points favoring the growth of mossy and/or dendritic Na. Currently, 3D electrode hosts can be divided into three categories based on substrate materials and composition: carbon-based, metal-based, and their composite frameworks. Despite their distinct microstructures, compositions, and performance advantages, the common objectives of this strategic approach is to enhance the electrochemical deposition behavior of sodium ions by increasing the nucleation sites and reducing the local current density, which collectively contribute to an improved performance of AFSMBs.

Typical metal-based current collectors, *e.g.*, Zn, Cu, and α-brass, were primarily screened for AFSMBs, as schematically illustrated in Fig. 15a.[151] Due to the crystallographic incompatibility between Cu and Na metal, Cu foils demonstrated worse CEs and cycling stability with large nucleation overpotentials, while Zn performed as the most suitable current collector material, delivering superior cycling stability with an average CE up to 98.9%. To improve the feasibility of Cu-based current collector, a Cu nanowire-reinforced 3D Cu foam current

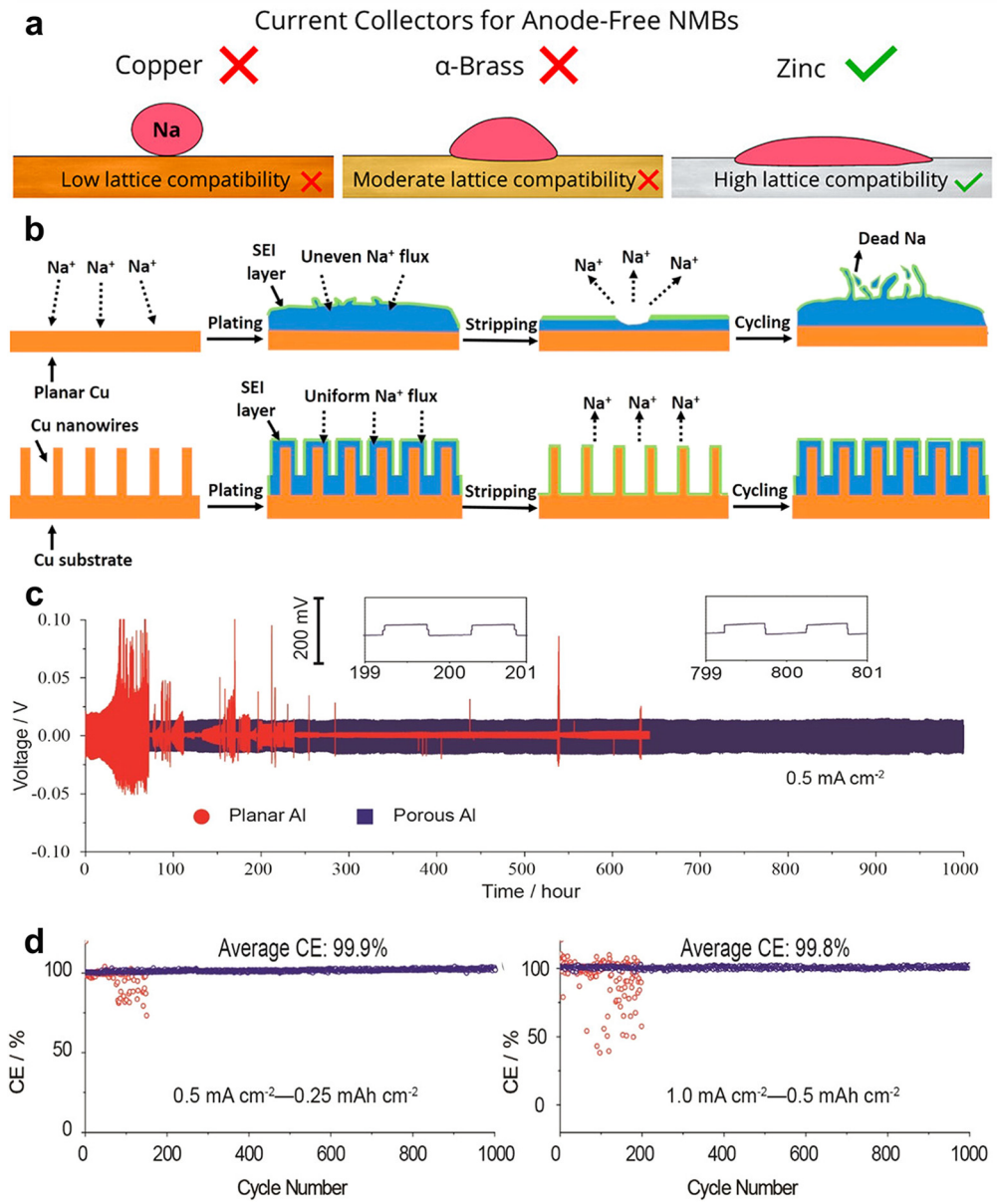

Fig. 15 (a) General evaluations of Na deposition on Cu, α-brass, and Zn current collectors, respectively, for AFSMBs. Reproduced with permission.[151] Copyright 2023 American Chemical Society. (b) Schematic illustration of the Na plating processes on planar Cu foil and CuNW-Cu substrate. Reproduced with permission.[152] Copyright 2018 Elsevier. (c) Galvanostatic cycling of symmetric Na@planar Al/Na and Na@porous Al/Na cells. The current density was fixed at 0.5 mA cm^{-2} with each cycle set to 1 h. (d) CE recorded during the first 1000 cycles of planar and porous Al with Na deposited amount of 0.25 mA h cm^{-2} at 0.5 mA cm^{-2} and 0.5 mA h cm^{-2} at 1 mA cm^{-2}. Reproduced with permission.[30] Copyright 2017 American Chemical Society.

collector (CuNW-Cu) was reported.[152] As depicted in Fig. 15b, the *in situ* grown Cu nanowires offer a multitude of active nucleation sites, which increase the current collector's surface area for reducing the local current density. This design enhances the diffusion of Na^+ ions across the electrode/electrolyte interface and equalizes the distribution of Na^+ flux. The same functionality was also observed in Al-based current collector system.[30] In addition to the cost-effectiveness and reduced weight compared to Cu current collector, the interconnected porous structure of Al-based current collectors demonstrated the capability to endure over 1000 Na stripping–plating cycles with minimal and stable voltage hysteresis and high average CE over 99.9% as depicted in Fig. 15c and d. This advancement is instrumental in enhancing the cyclability and efficiency of sodium deposition process by architecture design of the current collector, bringing the practical application of high-energy AFSMBs.

As reported, the carbon-based materials are widely used as hosting layers by modulating the deposition behavior of Na^+ on the conventional Al or Cu current collectors due to their high sodium affinity, electron conductivity and chemical stability. The direct use of porous carbon frameworks as current collectors offer a promising solution for sodium deposition in anode-

free batteries. For example, a 3D flexible commercial carbon felt can be employed as a host for sodium metal anode.[153] By further optimization, a 3D carbon-based sodiophilic substrate was fabricated by decorating silver (Ag) on carbon cloth through a facile thermal evaporation deposition method, which was then employed as anode current collector for AFSMB (Fig. 16a).[29] Theoretical simulations have demonstrated a preference for sodium ions to bind with Ag to form a Na–Ag network, thus effectively improving the Na plating/stripping reversibility by contributing to the formation of a thin and uniform SEI. The AFSMB employing such an anode current collector and a Prussian white cathode (Fig. 16b) delivered a capacity retention of approximately 56% after 800 cycles at 0.5C with a relatively slow capacity decay of 0.055% per cycle (Fig. 16c). Moreover, Kandula *et al.* designed a mechanically resilient MXene/CNT nano-accordion framework that serves as an efficient anode host for AFSMB (Fig. 16d).[40] The synergistic exposure of sodiophilic surface functional groups on the MXene nanoplates and CNTs provide an increased micro-sized porosity offering plenty of Na nucleation sites, allowing rapid and uniform Na plating/stripping. Besides, the high mechanical flexibility of the nano-accordion structure, stemming from the strong adhesion between MXene and CNT surfaces, enables the MXene/CNT nano-accordion frameworks to retain their structural integrity with minimal volume changes even under intensive stripping/plating process in high areal capacity. These benefits allow the anode-free full-cell coupled with a carbon coated $Na_3V_2(PO_4)_3$ cathode to run for the long-term cycle stability over 5000 cycles at 5.0C and 10.0C without failure (Fig. 16e), respectively.

Functionalization with inorganic species such as Sn,[41] CuP_3,[154] or $ZnIn_2S_4$[155] with an ultraconformal coating layer and sodiophilic properties may also promote more uniform Na nucleation and deposition. However, the use of 3D porous current collectors simultaneously increases the electrode in direct contact with the electrolyte and burdens Na consumption. Meanwhile, the mechanisms underlying the impact of the current collector geometry, material properties, surface energy, and mechanical characteristics on Na plating/stripping in practical applications still need further investigation.

4.4. Electrochemical modulations toward nucleation/diffusion kinetics

Regarding cell configuration, the operating protocols can influence the sodium deposition behavior and the overall cell performance. Approaches that have been widely employed in anode-free lithium batteries, taking into account variables such as temperature,[156] applied pressure,[157] and test parameters *e.g.*, cut-off voltage,[157] can be similarly extended to AFSMBs. External pressure, in particular, plays a vital role for cycle life in various cell configurations.[157] Applying pressure to the cell can influence the diffusion kinetics by

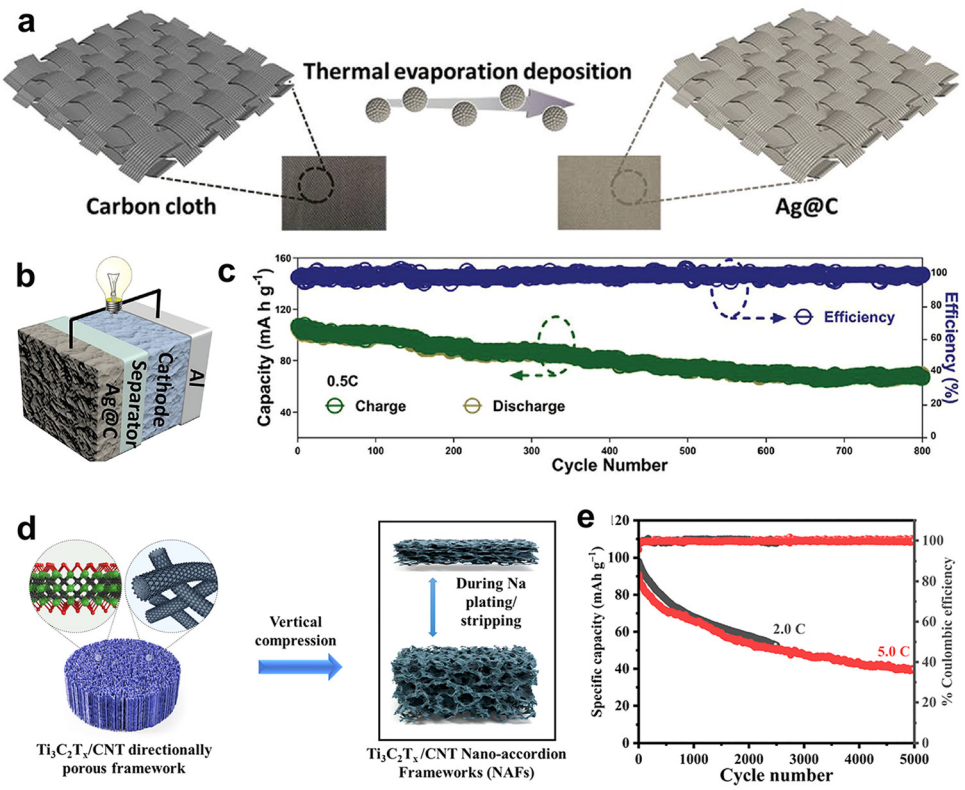

Fig. 16 (a) Schematic representation illustrating the deposition of Ag on a carbon cloth. (b) Schematic diagram of AFSMB configurations using Ag@C as anode current collector. (c) Long-term cycling performance of AFSMB at 0.5C within 2–4.2 V. Reproduced with permission.[29] Copyright 2021 Wiley-VCH GmbH. (d) Schematic illustration of the resilient $Ti_3C_2T_x$/CNT nano-accordion frameworks. (e) Cyclic stability plots of AFSMB. Reproduced with permission.[40] Copyright 2023 Elsevier.

reducing the interfacial resistance and enhancing the contact between the electrodes and the electrolyte, leading to enhanced performance.[158] Coin cells are the most widely used setups in laboratories considering their ease of assembly and reproducibility.[159,160] The applied pressure in a coin cell is typically adjusted by using additional spacers or a spring. It has been demonstrated that the use of an extra spacer in anode-free coin cell contributed to a superior performance, resulting in more homogenous metal deposition with both lower bulk and charge transfer resistances.[161] In the more practical pouch cells, the application of a compressive stack pressure enhances the contact between different cell components, which minimizes the internal and interface resistance.[162,163] For example, a split pouch cell (Na‖Cu, >10 cm^2) demonstrates the low hysteresis at moderate pressure ($\sim$185 kPa), while the extended cycle life can be achieved when increasing the pressure to 742 kPa, indicating that high pressures can enable the non-dendritic sodium deposition by proper contact between electrodes.[164] The increased pressure greatly suppressed the formation of needle-like or star-shaped sodium deposits, consequently decreasing the reduced surface area involved in side reactions as well as SEI formation. However, the effects on other parameters such as gas evolution, SEI growth, and dendrite formation are still not clear. Further research and optimization of pressure-induced effects are essential to fully realize the potential of this modulation strategy.

Electrochemical modulations play a crucial role in enhancing the nucleation and diffusion kinetics in anode-free batteries. The cut-off voltage is another key parameter indicating the electrochemical performance of full cell or anode-free batteries.[165] J. Dahn *et al.*[33] observed that adjusting the lower cut-off voltage from 3.6 V to 1.25 V can significantly affect the cycling behavior and CE of anode free batteries. In particular, the cells discharged to 3.6 V displayed sharp fading after 5–10 cycles, although offering high initial CE above 99.8%, which did not occur in the cells discharged to 1.25 V. While further examination is required to fully understand the underlying mechanisms of these effects. Additionally, the adjustment of the cut-off voltage range can regulate the redox reactions.[31] For example, a $Na_3V_2(PO_4)_3$ (Na_3VP) cathode can be presodiated and transformed into $Na_5V_2(PO_4)_3$ (Na_5VP), which serves as a suitable sodium replenisher to compensate the sodium loss, and more importantly allows a reversible three-electron redox reaction in a wide voltage range of 1.0–3.8 V, as illustrated in Fig. 17a. Fig. 17b illustrates the galvanostatic charge–discharge (GCD) profiles of the Na5VP‖Al/C cell, which reveal two notable plateaus at 0.35 V and 1.7 V *versus* Na/Na$^+$ during the initial charging cycle. These voltage plateaus are associated with the phase transitions that occur as the pre-sodiated sodium is extracted from the Na_5VP electrode material. The widened voltage range can unlock a high energy density of 400 W h kg^{-1} in the anode-free sodium battery that uses Al/C as an anode current collector, enabling a superior cycling performance compared with a narrower cut-off voltage range of 3.0–3.8 V (Fig. 17c). Similar performance enhancements have been observed in recent work by Hu *et al.*[37] The cycling retention is increased from 82% after 200 cycles to 84% after 260 cycles when the upper-cut-off voltage is reduced from 4.0 V to 3.8 V. These findings indicate the significance of test prototype modulation in optimizing the performance of anode-free batteries, which should be explored further to enhance both energy density and cycling stability of AFSMBs for practical applications.

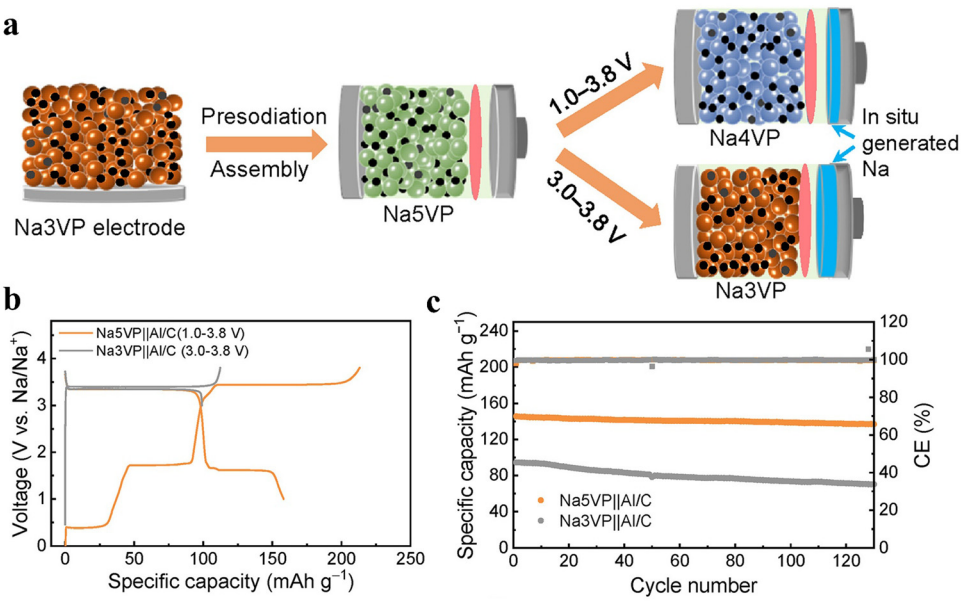

Fig. 17 (a) Illustration of presodiation, assembly, and operation of AFSMB in two different voltage windows, (b) initial GCD profiles and (c) cyclic performance of Na_5VP‖Al cells within different voltage windows (1.0–3.8 and 3.0–3.8 V). Reproduced with permission.[31] Copyright 2021 Wiley-VCH GmbH.

5. Summary and perspectives

Anode-free sodium metal batteries (AFSMBs) are a cutting-edge battery technology that promises high energy density, reduced manufacturing costs, and enhanced safety. However, they face significant challenges such as limited sodium availability, the formation of inactive sodium, and issues with the SEI formation, which collectively undermine cycle performance, hindering their practical application. In this context, optimizing the utilization of sodium ions is crucial for prolonging the lifespan and enhancing the efficiency of AFSMBs. Herein, the major challenges and fundamental issues related to the performance of AFSMBs have been summarized, with a specific emphasis on the recent advancements in electrolyte and interphase optimization aimed at enhancing the long-term cycling stability and CEs, as depicted in Fig. 18.

Despite the breakthroughs in electrolytes and interphase designs, there are still considerable challenges to overcome to achieve stable, long-term cycling performance for AFSMBs. The primary issues hindering the practical application of AFSMBs are: (i) the conventional planar anode current collector struggles to regulate the morphology of sodium plating and stripping, in which the spatial confinement can lead to the build-up of interfacial stress, potentially causing structural failure and the formation of dead sodium; (ii) uncontrolled side reactions and the persistent formation of the SEI layer stem from the thermodynamic instability of metallic sodium, which will gradually consume electrolyte and lead to capacity loss upon cycling; (iii) high nucleation energy barriers hinder the efficient sodium ion transport and contribute to uneven sodium deposition in AFSMBs due to poor affinity between the inert substrate and metallic sodium. All these issues can be potentially addressed by regulating the sodium behaviors at the electrolyte/current collector interface. Particularly, the development of solid-state AFSMBs requires robust solid–solid interface contact between solid electrolytes and current collectors. Although the strategies discussed have contributed to extended AFSMB lifespan, further enhancements are essential for achieving more stable and reliable performance. Future developments in the following areas are fundamental for realizing AFSMBs with high energy density, extended cycle life, and improved safety.

(1) Deep understanding of electrolyte-derived SEI and Na deposition mechanisms.

The deposition of sodium metal on inert current collectors is a complex process, significantly influenced by the formation of the SEI layer. Characterizing the SEI in real-time without altering its state is challenging, but essential for understanding its impact on Na deposition behavior. Theoretical methods, including molecular dynamics simulations and quantum mechanical calculations, are pivotal for elucidating the intricate interfacial reactions between electrolyte constituents and electrode materials. These tools help us grasp atomic-scale electronic configurations and reactive potentials, while thermodynamic and kinetic models forecast the SEI's evolution. DFT and *ab initio* molecular dynamics (AIMD) simulations offer detailed insights into the structural and dynamic behaviors of electrolytes. Empirical data from spectroscopic techniques further enrich our understanding by revealing the SEI's chemical architecture and physicochemical attributes. Continuum models such as pseudo-2D (P2D), pseudo-3D (P3D) multiscale, and 4D-resolved models, simulate the bulk electrochemical performance, which are often integrated with physical degradation models to account for SEI formation and growth.[166–168] This synergy between theory and experiment aids in electrolyte optimization, SEI engineering, additive selection,

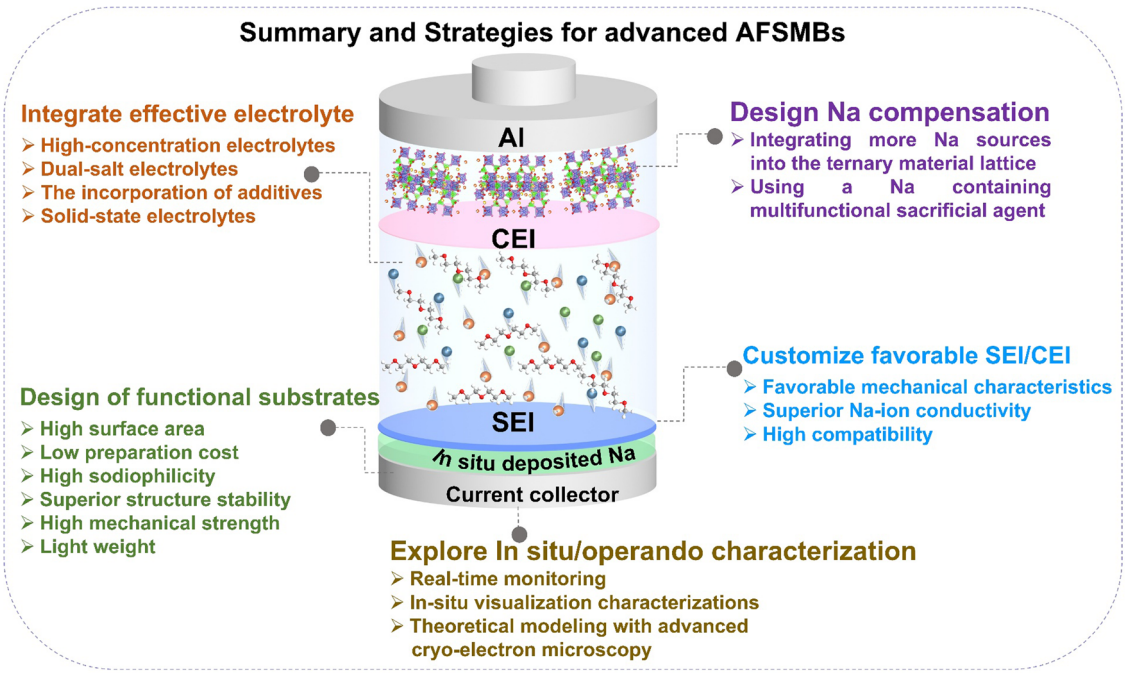

Fig. 18 Summary and perspectives on research directions of AFSMBs.

and the superior compatibility of electrolytes and SEI, paving the way for robust and efficient battery technologies.

The integration of advanced real-time monitoring with *in situ* visualization techniques significantly enhances the understanding of sodium desolvation, nucleation, plating, stripping, and SEI formation during battery cycling. Advanced operando experiments, particularly cryo-electron microscopy, provide profound insights into these processes. Techniques like cryo-SEM, HR-TEM, atomic force microscopy, and various spectroscopies deliver atomic-level data on SEI and interfacial evolution.[169,170] However, the true value lies in real-time operando techniques such as SANS/WANS, quasi-elastic neutron scattering, neutron reflectometry, and terahertz spectroscopy, which offer a dynamic view of the SEI.[167,171] These methods, in concert with computational calculations and simulations, enable a comprehensive understanding of SEI and sodium deposition mechanisms. By merging these advanced techniques with theoretical models, we can predict and control SEI behavior, driving the development of efficient and sustainable battery technologies for the next generation of high-performing energy storage systems.

(2) Efficient sodium source replenishment and pre-sodiation technologies.

Developing Na compensation strategies in AFSMBs involves innovative approaches from both electrolyte and cathode sides to ensure stable operation and longevity. Formulating electrolytes that can provide a steady Na^+ supply, such as the use of high concentrated electrolyte and sacrificial additives compensating the Na loss from the inevitable SEI formation and other side reactions. The incorporation of sacrificial agents in electrolytes that contain sodium and serve to replenish the sodium loss can significantly enhance the efficiency and cycling stability of AFSMBs. Currently, the most commonly used sacrificial agents, including $Na_2C_4O_4$,[172] $Na_2C_2O_4$,[173] Na_2S,[174] Na_3P,[175] NaN_3,[176] are insoluble in the conventional liquid electrolytes. Thus, they are added into the composite cathode. However, safety concerns are paramount with materials like Na_3P and NaN_3, respectively, prone to flammability and explosion. Additionally, although compounds such as Na_2CO_3 hold high theoretical capacities, their actual usable capacity is limited. The need for catalysts to reduce the high desodiation potentials of other compounds like sodium thiophosphate (Na_3PS_3O) and $Na_2C_2O_4$ further complicates the manufacturing process, driving up costs. In this context, molecular design of sacrificial sodium salts with low desodiation potential, high-capacity, solubility in the electrolyte, and insulating/gas byproduct-free should be devoted to promoting the reversible capacity and cycling performance of AFSMBs. Considering the fact that the cathodes provide the only sodium source in anode-free batteries, another promising strategy involves enhancing the cathode material itself to contain additional Na sources. This can be accomplished by pre-sodiation treatment with more sodium into the lattice, effectively creating a sodium reservoir that compensates for the initial sodium plating and any subsequent loss during cycling. Moreover, developing sodium-rich cathode materials like layered oxides, polyanionic compounds, and Prussian blue analogs is also pivotal for harboring additional sodium ions, which could be realized by precise crystal engineering from advanced synthesis. By integrating these strategies, AFSMBs can potentially achieve a more balanced sodium supply and contribute to improved performance. Further research and development in sodium source replenishment and pre-sodiation technologies *via* electrolyte modification are essential to fully attain the benefits of high energy and long-term cycling in AFSMBs.

(3) Optimization of primary battery structure and test conditions.

Optimizing primary battery structure and related accessories is crucial for boosting functionality, efficiency, and safety. Key strategies include refining compatibility of electrode reaction mechanisms, optimizing cell configurations for desired voltage and capacity, and employing separators without short circuits. Structuring the internal layout of a battery is required to optimize the series and parallel connections of cells for achieving desired voltage and capacity. Meanwhile, using a modular design approach enhances the battery's resilience to internal strain, particularly in anode-free batteries. This design permits the necessary expansion and contraction of electrodes without compromising the structural integrity of the battery. By allowing for such movement, the modular design helps to distribute mechanical stress more evenly, consequently reducing the risk of deformation or damage to the electrode structure. Moreover, functionalized separators that allow efficient ion transport and affect the morphological evolution of Na deposits can remarkably improve the CE and lifespan of SMBs, while the design and working mechanisms of the state-of-the-art separators were rarely presented and discussed in AFSMBs.[177,178]

Test conditions also play a significant role in improving the cycling performance and energy density of AFSMBs, with factors such as cut-off voltage, working current density, surrounding temperature, and stacking pressure. A lower cut-off voltage may improve cycle stability but also reduce energy density, necessitating research into strategies that maintain stability at higher voltage to achieve greater energy densities. Typically, AFSMBs operate at lower current densities for better capacity and stability, though this can extend operation times and limit practicality. Fortunately, recent studies suggest that using lower charging currents and higher discharging currents can enhance cycling stability, emphasizing that the charging-to-discharging rate ratio is more impactful on cycle life than absolute current densities. Optimizing these rates could significantly extend the practical applications of AFSMBs. Additionally, broadening the operational temperature range could further expand the real-world practicality of these batteries. By refining these test conditions, AFSMBs can be tailored for a wider range of applications without sacrificing performance or safety.

(4) Developing high-energy batteries under cryogenic conditions.

The development of high-energy-density anode-free batteries for cryogenic conditions is impeded by challenges such as poor metal plating/stripping reversibility and unstable SEI. Kinetically, the performance at temperatures below -20 °C

faces significant challenges particularly due to kinetic barriers of ion transport, cation desolvation at the electrode/electrolyte interface. Meanwhile, the desolvation of Na^+ ions is particularly sensitive to low temperatures, leading to increased charge transfer resistance and the formation of undesirable sodium dendrites at the SEI. The Na^+ desolvation is influenced by the competitive coordination among cations, anions, and solvent molecules, indicating that modulating the solvation chemistry within the electrolyte is key to controlling the interfacial dynamics of Na^+ at low temperatures. Therefore, the exploration of weakly solvating solvents presents a promising direction for AFSMBs, as they can reduce desolvation energy and allow a smaller number of solvent molecules to occupy the inner solvation sheath. Additionally, interface engineering through additives and surface modifications aim to foster a stable and thin SEI, while fundamental research delves into the low-temperature electrochemical behavior, metal deposition mechanisms, and SEI formation. A comprehensive understanding of the solvation involving Na^+, anions, and solvent molecules and interfacial reactions is critical for low-temperature AFSMBs. Nevertheless, by tackling these issues through a combination of electrode material innovation, electrolyte engineering, and design optimization, it is possible to develop high-energy-density anode-free batteries to operate effectively in cryogenic conditions.

In summary, the successful implementation of AFSMBs relies heavily on a synergistic integration of various modification strategies, including the optimization of current collectors, interfacial engineering to stabilize the SEI, the formulation of electrolytes with enhanced ionic conductivity and the compatibility with sodium metal, the establishment of operational protocols that ensure safe and efficient functioning, and the designs of cathodes that can withstand the stresses of low-temperature operation. The collective goal is to unlock the full potential of AFSMBs, propelling their evolution as a reliable, safe, and high-energy-density energy storage solution for practical applications, especially under cryogenic conditions.

Data availability

No primary research results, software or code have been included and no new data were generated or analysed as part of this review.

Conflicts of interest

There are no conflicts to declare.

Acknowledgements

H. L., F. W., and J. W. contributed equally to this work. This research was supported by the National Natural Science Foundation of China (52307236, 52377214), the China Postdoctoral Science Foundation (2023M730885, 2024M752502), the Postdoctoral Science Foundation of Heilongjiang Province (LBH-Z23197) and the Opening funding from Key Laboratory of Engineering Dielectrics and Its Application (Harbin University of Science and Technology) (No. KFM202507, Ministry of Education). Dr J. Wang thanks the fellowship supported by the Alexander von Humboldt Foundation, and the basic funding of the Helmholtz Association.

References

1 Z. Yang, J. Zhang, M. C. Kintner-Meyer, X. Lu, D. Choi, J. P. Lemmon and J. Liu, *Chem. Rev.*, 2011, **111**, 3577–3613.
2 J. Wang, J. Zhang, Y. Zhang, H. Li, P. Chen, C. You, M. Liu, H. Lin and S. Passerini, *Adv. Mater.*, 2024, **36**, e2402792.
3 J. Wang, J. Zhang, S. Duan, L. Jia, Q. Xiao, H. Liu, H. Hu, S. Cheng, Z. Zhang, L. Li, W. Duan, Y. Zhang and H. Lin, *Nano Lett.*, 2022, **22**, 8008–8017.
4 J. Wang, J. Zhang, J. Wu, M. Huang, L. Jia, L. Li, Y. Zhang, H. Hu, F. Liu, Q. Guan, M. Liu, H. Adenusi, H. Lin and S. Passerini, *Adv. Mater.*, 2023, **35**, e2302828.
5 H. Li, J. Wang, J. Zhang, L. Jia, H. Qu, Q. Guan, H. Zhang and H. Lin, *Green Chem.*, 2024, **26**, 10366–10382.
6 P. Loganathan, G. Naidu and S. Vigneswaran, *Environ. Sci.: Water Res. Technol.*, 2017, **3**, 37–53.
7 V. Christoph, B. Daniel, W. A. Marcel and P. Stefano, *Nat. Rev. Mater.*, 2018, **3**, 18013.
8 H. Moriwake, A. Kuwabara, C. A. J. Fisher and Y. Ikuhara, *RSC Adv.*, 2017, **7**, 36550–36554.
9 Z. L. Xu, G. Yoon, K. Y. Park, H. Park, O. Tamwattana, S. Joo Kim, W. M. Seong and K. Kang, *Nat. Commun.*, 2019, **10**, 2598.
10 G. Chang, Y. Zhao, L. Dong, D. P. Wilkinson, L. Zhang, Q. Shao, W. Yan, X. Sun and J. Zhang, *J. Mater. Chem. A*, 2020, **8**, 4996–5048.
11 S. Fang, D. Bresser and S. Passerini, *Adv. Energy Mater.*, 2019, **10**, 1902485.
12 Z. Li, J. Ding and D. Mitlin, *Acc. Chem. Res.*, 2015, **48**, 1657–1665.
13 H. Wang, E. Matios, J. Luo and W. Li, *Chem. Soc. Rev.*, 2020, **49**, 3783–3805.
14 K. Chayambuka, G. Mulder, D. L. Danilov and P. H. L. Notten, *Adv. Energy Mater.*, 2018, **8**, 1800079.
15 J. Y. Hwang, S. T. Myung and Y. K. Sun, *Chem. Soc. Rev.*, 2017, **46**, 3529–3614.
16 Y. Fang, X. Y. Yu and X. W. D. Lou, *Angew. Chem., Int. Ed.*, 2017, **56**, 5801–5805.
17 B. Sun, P. Li, J. Zhang, D. Wang, P. Munroe, C. Wang, P. H. L. Notten and G. Wang, *Adv. Mater.*, 2018, **30**, 1801334.
18 H. Tian, Z. W. Seh, K. Yan, Z. Fu, P. Tang, Y. Lu, R. Zhang, D. Legut, Y. Cui and Q. Zhang, *Adv. Energy Mater.*, 2017, **7**, 1602528.
19 B. Y. Lee, E. Paek, D. Mitlin and S. W. Lee, *Chem. Rev.*, 2019, **119**, 5416–5460.
20 Y. Wang, Y. Wang, Y.-X. Wang, X. Feng, W. Chen, X. Ai, H. Yang and Y. Cao, *Chem*, 2019, **5**, 2547–2570.
21 C. Zhang, A. Wang, J. Zhang, X. Guan, W. Tang and J. Luo, *Adv. Energy Mater.*, 2018, **8**, 1802833.

22 Z. Lu, H. Yang, Q. H. Yang, P. He and H. Zhou, *Angew. Chem., Int. Ed.*, 2022, **61**, e202200410.
23 K. Lee, Y. J. Lee, M. J. Lee, J. Han, J. Lim, K. Ryu, H. Yoon, B. H. Kim, B. J. Kim and S. W. Lee, *Adv. Mater.*, 2022, **34**, 2109767.
24 Y. X. Wang, H. Dong, N. Katyal, H. C. Hao, P. C. Liu, H. Celio, G. Henkelman, J. Watt and D. Mitlin, *Adv. Mater.*, 2022, **34**, 2106005.
25 K. N. Shitaw, S. C. Yang, S. K. Jiang, C. J. Huang, N. A. Sahalie, Y. Nikodimos, H. H. Weldeyohannes, C. H. Wang, S. H. Wu, W. N. Su and B. J. Hwang, *Adv. Funct. Mater.*, 2020, **31**, 2006951.
26 J. Wang, L. Li, H. Hu, H. Hu, Q. Guan, M. Huang, L. Jia, H. Adenusi, K. V. Tian, J. Zhang, S. Passerini and H. Lin, *ACS Nano*, 2022, **16**, 17729–17760.
27 H. Dai, X. Gu, J. Dong, C. Wang, C. Lai and S. Sun, *Nat. Commun.*, 2020, **11**, 643.
28 Y. Kim, M. Kuenzel, D. Steinle, X. Dong, G.-T. Kim, A. Varzi and S. Passerini, *Energy Environ. Sci.*, 2022, **15**, 2610–2618.
29 H. Wang, Y. Wu, S. H. Liu, Y. Jiang, D. Shen, T. X. Kang, Z. Q. Tong, D. Wu, X. J. Li and C. S. Lee, *Small Methods*, 2021, **5**, 2001050.
30 S. Liu, S. Tang, X. Zhang, A. Wang, Q. H. Yang and J. Luo, *Nano Lett.*, 2017, **17**, 5862–5868.
31 J. Wu, C. Lin, Q. Liang, G. Zhou, J. Liu, G. Liang, M. Wang, B. Li, L. Hu, F. Ciucci, Q. Liu, G. Chen and X. Yu, *InfoMat*, 2022, **4**, e12288.
32 Y.-Y. Zhang, C.-H. Zhang, Y.-J. Guo, M. Fan, Y. Zhao, H. Guo, W.-P. Wang, S.-J. Tan, Y.-X. Yin, F. Wang, S. Xin, Y.-G. Guo and L.-J. Wan, *J. Am. Chem. Soc.*, 2023, **145**, 25643–25652.
33 M. Genovese, A. J. Louli, R. Weber, S. Hames and J. R. Dahn, *J. Electrochem. Soc.*, 2018, **165**, A3321–A3325.
34 S. Y. Hong, Y. Kim, Y. Park, A. Choi, N.-S. Choi and K. T. Lee, *Energy Environ. Sci.*, 2013, **6**, 2067–2081.
35 X. Zheng, L. Huang, X. Ye, J. Zhang, F. Min, W. Luo and Y. Huang, *Chem*, 2021, **7**, 2312–2346.
36 J. Hwang, A. N. Sivasengaran, H. Yang, H. Yamamoto, T. Takeuchi, K. Matsumoto and R. Hagiwara, *ACS Appl. Mater. Interfaces*, 2021, **13**, 2538–2546.
37 Y. Li, Q. Zhou, S. Weng, F. Ding, X. Qi, J. Lu, Y. Li, X. Zhang, X. Rong, Y. Lu, X. Wang, R. Xiao, H. Li, X. Huang, L. Chen and Y.-S. Hu, *Nat. Energy*, 2022, **7**, 511–519.
38 A. P. Cohn, N. Muralidharan, R. Carter, K. Share and C. L. Pint, *Nano Lett.*, 2017, **17**, 1296–1301.
39 C. Wang, Y. Zheng, Z.-N. Chen, R. Zhang, W. He, K. Li, S. Yan, J. Cui, X. Fang, J. Yan, G. Xu, D. Peng, B. Ren and N. Zheng, *Adv. Energy Mater.*, 2023, **13**, 2204125.
40 S. Kandula, E. Kim, C. W. Ahn, J. Lee, B. Yeom, S. W. Lee, J. Cho, H.-K. Lim, Y. Lee and J. G. Son, *Energy Storage Mater.*, 2023, **63**, 103024.
41 S. Li, H. Zhu, Y. Liu, Q. Wu, S. Cheng and J. Xie, *Adv. Mater.*, 2023, **35**, 2301967.
42 Y. Tian, Y. An, C. Wei, H. Jiang, S. Xiong, J. Feng and Y. Qian, *Nano Energy*, 2020, **78**, 105344.
43 W. Huang, C. Zhao, P. Wu, H. Yuan, W. E. Feng, Z. Y. Liu, Y. Lu, S. Sun, Z. H. Fu, J. K. Hu, S. J. Yang, J. Q. Huang and Q. Zhang, *Adv. Energy Mater.*, 2022, **12**, 2201044.
44 Q. Ni, Y. Yang, H. Du, H. Deng, J. Lin, L. Lin, M. Yuan, Z. Sun and G. Sun, *Batteries*, 2022, **8**, 272.
45 T. Yang, D. Luo, Y. Liu, A. Yu and Z. Chen, *iScience*, 2023, **26**, 105982.
46 J.-G. Zhang, *Nat. Energy*, 2019, **4**, 637–638.
47 H. Li, H. Zhang, F. Wu, M. Zarrabeitia, D. Geiger, U. Kaiser, A. Varzi and S. Passerini, *Adv. Energy Mater.*, 2022, **12**, 2202293.
48 R. Zhuang, X. Zhang, C. Qu, X. Xu, J. Yang, Q. Ye, Z. Liu, S. Kaskel, F. Xu and H. Wang, *Sci. Adv.*, 2023, **9**, eadh8060.
49 B. Sun, P. Xiong, U. Maitra, D. Langsdorf, K. Yan, C. Wang, J. Janek, D. Schroder and G. Wang, *Adv. Mater.*, 2020, **32**, 1903891.
50 A. Pei, G. Zheng, F. Shi, Y. Li and Y. Cui, *Nano Lett.*, 2017, **17**, 1132–1139.
51 Y. Xu, A. S. Menon, P. P. R. M. L. Harks, D. C. Hermes, L. A. Haverkate, S. Unnikrishnan and F. M. Mulder, *Energy Storage Mater.*, 2018, **12**, 69–78.
52 E. Matios, H. Wang, C. Wang and W. Li, *Ind. Eng. Chem. Res.*, 2019, **58**, 9758–9780.
53 T. T. Beyene, H. K. Bezabh, M. A. Weret, T. M. Hagos, C.-J. Huang, C.-H. Wang, W.-N. Su, H. Dai and B.-J. Hwang, *J. Electrochem. Soc.*, 2019, **166**, A1501–A1509.
54 Q. Cheng, A. Li, N. Li, S. Li, A. Zangiabadi, T.-D. Li, W. Huang, A. C. Li, T. Jin, Q. Song, W. Xu, N. Ni, H. Zhai, M. Dontigny, K. Zaghib, X. Chuan, D. Su, K. Yan and Y. Yang, *Joule*, 2019, **3**, 1510–1522.
55 Y. Zhang, T.-T. Zuo, J. Popovic, K. Lim, Y.-X. Yin, J. Maier and Y.-G. Guo, *Mater. Today*, 2020, **33**, 56–74.
56 S. Kim, C. Jung, H. Kim, K. E. Thomas-Alyea, G. Yoon, B. Kim, M. E. Badding, Z. Song, J. Chang, J. Kim, D. Im and K. Kang, *Adv. Energy Mater.*, 2020, **10**, 1903993.
57 S. Tang, Z. Qiu, X.-Y. Wang, Y. Gu, X.-G. Zhang, W.-W. Wang, J.-W. Yan, M.-S. Zheng, Q.-F. Dong and B.-W. Mao, *Nano Energy*, 2018, **48**, 101–106.
58 J. Jung, D. Y. Hwang, I. Kristanto, S. K. Kwak and S. J. Kang, *J. Mater. Chem. A*, 2019, **7**, 9773–9781.
59 G. M. Hobold, J. Lopez, R. Guo, N. Minafra, A. Banerjee, Y. Shirley Meng, Y. Shao-Horn and B. M. Gallant, *Nat. Energy*, 2021, **6**, 951–960.
60 Z. Hu, L. Liu, X. Wang, Q. Zheng, C. Han and W. Li, *Adv. Funct. Mater.*, 2024, **34**, 2313823.
61 Y. Zhao, K. R. Adair and X. L. Sun, *Energy Environ. Sci.*, 2018, **11**, 2673–2695.
62 J. Luo, C. Wang, H. Wang, X. Hu, E. Matios, X. Lu, W. Zhang, X. Tao and W. Li, *Adv. Funct. Mater.*, 2018, **29**, 1805946.
63 B. Wu, C. Chen, L. H. J. Raijmakers, J. Liu, D. L. Danilov, R.-A. Eichel and P. H. L. Notten, *Energy Storage Mater.*, 2023, **57**, 508–539.
64 D. Aurbach, *J. Power Sources*, 2000, **89**, 206–218.
65 K. Pfeifer, S. Arnold, J. Becherer, C. Das, J. Maibach, H. Ehrenberg and S. Dsoke, *ChemSusChem*, 2019, **12**, 3312–3319.

66 J. Lee, J. Kim, S. Kim, C. Jo and J. Lee, *Mater. Adv.*, 2020, **1**, 3143–3166.
67 L. Schafzahl, I. Hanzu, M. Wilkening and S. A. Freunberger, *ChemSusChem*, 2016, **10**, 401–408.
68 K. M. Abraham, J. L. Goldman and D. I. Natwig, *J. Electrochem. Soc.*, 1982, **129**, 2404–2409.
69 K. M. Abraham, D. M. Pasquariello and F. J. Martin, *J. Electrochem. Soc.*, 1986, **133**, 661.
70 I. Yoshimatsu, T. Hirai and J.-I. Yamaki, *J. Electrochem. Soc.*, 1988, **135**, 2422.
71 K. Xu, Y. Lam, S. S. Zhang, T. R. Jow and T. B. Curtis, *J. Phys. Chem. C*, 2007, **111**, 7411–7421.
72 A. von Wald Cresce, O. Borodin and K. Xu, *J. Phys. Chem. C*, 2012, **116**, 26111–26117.
73 B. Jache and P. Adelhelm, *Angew. Chem., Int. Ed.*, 2014, **53**, 10169–10173.
74 M. Goktas, C. Bolli, E. J. Berg, P. Novák, K. Pollok, F. Langenhorst, M. V. Roeder, O. Lenchuk, D. Mollenhauer and P. Adelhelm, *Adv. Energy Mater.*, 2018, **8**, 1702724.
75 L. Seidl, N. Bucher, E. Chu, S. Hartung, S. Martens, O. Schneider and U. Stimming, *Energy Environ. Sci.*, 2017, **10**, 1631–1642.
76 H. Kim, K. Lim, G. Yoon, J. H. Park, K. Ku, H. D. Lim, Y. E. Sung and K. Kang, *Adv. Energy Mater.*, 2017, **7**, 1700418.
77 Y. Liu, B. V. Merinov and W. A. Goddard, *Proc. Natl. Acad. Sci. U. S. A.*, 2016, **113**, 3735–3739.
78 R. Cao, K. Mishra, X. Li, J. Qian, M. H. Engelhard, M. E. Bowden, K. S. Han, K. T. Mueller, W. A. Henderson and J.-G. Zhang, *Nano Energy*, 2016, **30**, 825–830.
79 Z. W. Seh, J. Sun, Y. Sun and Y. Cui, *ACS Cent. Sci.*, 2015, **1**, 449–455.
80 A. Rudola, S. R. Gajjela and P. Balaya, *Electrochem. Commun.*, 2018, **86**, 157–160.
81 H. Sun, G. Zhu, X. Xu, M. Liao, Y.-Y. Li, M. Angell, M. Gu, Y. Zhu, W. H. Hung, J. Li, Y. Kuang, Y. Meng, M.-C. Lin, H. Peng and H. Dai, *Nat. Commun.*, 2019, **10**, 3302.
82 H. Zhang, I. Hasa, D. Buchholz, B. Qin, D. Geiger, S. Jeong, U. Kaiser and S. Passerini, *NPG Asia Mater.*, 2017, **9**, e370.
83 S. A. Ferdousi, L. A. O'Dell, M. Hilder, A. J. Barlow, M. Armand, M. Forsyth and P. C. Howlett, *ACS Appl. Mater. Interfaces*, 2021, **13**, 5706–5720.
84 D. Monti, E. Jónsson, M. R. Palacín and P. Johansson, *J. Power Sources*, 2014, **245**, 630–636.
85 B. Song, X. Xiong, Y. Peng, X. Liu, W. Gao, T. Wang, F. Wang, Y. Ma, Y. Zhong, X.-B. Cheng, Z. Zhu, J. He and Y. Wu, *Adv. Energy Mater.*, 2024, **14**, 2401407.
86 K. Matsumoto, J. Hwang, S. Kaushik, C.-Y. Chen and R. Hagiwara, *Energy Environ. Sci.*, 2019, **12**, 3247–3287.
87 M. Armand, F. Endres, D. R. MacFarlane, H. Ohno and B. Scrosati, *Nat. Mater.*, 2009, **8**, 621–629.
88 X. Liu, A. Mariani, H. Adenusi and S. Passerini, *Angew. Chem., Int. Ed.*, 2023, **62**, e202219318.
89 X. Liu, C. Xu, H. Adenusi, Y. Wu and S. Passerini, *Acc. Chem. Res.*, 2025, **58**, 354–365.
90 M. Li, C. Wang, Z. Chen, K. Xu and J. Lu, *Chem. Rev.*, 2020, **120**, 6783–6819.
91 O. Borodin, J. Self, K. A. Persson, C. Wang and K. Xu, *Joule*, 2020, **4**, 69–100.
92 Z. Zhang, J. Wang, H. Qin, B. Zhang, H. Lin, W. Zheng, D. Wang, X. Ji and X. Ou, *ACS Nano*, 2024, **18**, 2250–2260.
93 A. Sun, H. F. Tu, Z. G. Sun, Z. G. He, Y. C. Wang, J. Wang, Y. T. Zheng, F. Y. Zhu, L. Wang, F. Mushtaq, P. Xue, J. Liu and M. A. Liu, *ACS Energy Lett.*, 2024, **9**, 2545–2553.
94 N. Dubouis, T. Marchandier, G. Rousse, F. Marchini, F. Fauth, M. Avdeev, A. Iadecola, B. Porcheron, M. Deschamps, J. M. Tarascon and A. Grimaud, *Nat. Mater.*, 2021, **20**, 1545–1550.
95 J. Qian, B. D. Adams, J. Zheng, W. Xu, W. A. Henderson, J. Wang, M. E. Bowden, S. Xu, J. Hu and J. G. Zhang, *Adv. Funct. Mater.*, 2016, **26**, 7094–7102.
96 J. Sun, L. A. O'Dell, M. Armand, P. C. Howlett and M. Forsyth, *ACS Energy Lett.*, 2021, **6**, 2481–2490.
97 D. A. Rakov, F. Chen, S. A. Ferdousi, H. Li, T. Pathirana, A. N. Simonov, P. C. Howlett, R. Atkin and M. Forsyth, *Nat. Mater.*, 2020, **19**, 1096–1101.
98 S. Wan, K. Song, J. Chen, S. Zhao, W. Ma, W. Chen and S. Chen, *J. Am. Chem. Soc.*, 2023, **145**, 21661–21671.
99 J. Zheng, S. Chen, W. Zhao, J. Song, M. H. Engelhard and J.-G. Zhang, *ACS Energy Lett.*, 2018, **3**, 315–321.
100 Z. Lu, H. Yang, G. Wu, P. Shan, H. Lin, P. He, J. Zhao, Y. Yang and H. Zhou, *Adv. Mater.*, 2024, **36**, 2404569.
101 J. Alvarado, M. A. Schroeder, T. P. Pollard, X. Wang, J. Z. Lee, M. Zhang, T. Wynn, M. Ding, O. Borodin, Y. S. Meng and K. Xu, *Energy Environ. Sci.*, 2019, **12**, 780–794.
102 R. R. Vaidyula, M. H. Nguyen, J. A. Weeks, Y. Wang, Z. Wang, K. Kawashima, A. G. Paul-Orecchio, H. Celio, A. Dolocan, G. Henkelman and C. B. Mullins, *Adv. Mater.*, 2024, **36**, 2312508.
103 R. Mogensen, D. Brandell and R. Younesi, *ACS Energy Lett.*, 2016, **1**, 1173–1178.
104 J. Moon, D. O. Kim, L. Bekaert, M. Song, J. Chung, D. Lee, A. Hubin and J. Lim, *Nat. Commun.*, 2022, **13**, 4538.
105 H. Zhang, Z. Zeng, F. Ma, Q. Wu, X. Wang, S. Cheng and J. Xie, *Angew. Chem., Int. Ed.*, 2023, **62**, e202300771.
106 X. Liu, L. Guo, Z. Zhang, J. Wang, H. Lin, G. Li, X. Ou, D. Wang and W. Zheng, *Adv. Funct. Mater.*, 2025, **35**, 2408525.
107 L. Hu, J. Deng, Y. Lin, Q. Liang, B. Ge, Q. Weng, Y. Bai, Y. Li, Y. Deng, G. Chen and X. Yu, *Adv. Mater.*, 2024, **36**, 2312161.
108 D. Ruan, L. Tan, S. Chen, J. Fan, Q. Nian, L. Chen, Z. Wang and X. Ren, *JACS Au*, 2023, **3**, 953–963.
109 D. Wu, C. Zhu, M. Wu, H. Wang, J. Huang, D. Tang and J. Ma, *Angew. Chem., Int. Ed.*, 2022, **61**, e202214198.
110 X. Zhou, Y. Huang, B. Wen, Z. Yang, Z. Hao, L. Li, S.-L. Chou and F. Li, *Proc. Natl. Acad. Sci. U. S. A.*, 2024, **121**, e2316914121.
111 M. Goktas, C. Bolli, J. Buchheim, E. J. Berg, P. Novák, F. Bonilla, T. Rojo, S. Komaba, K. Kubota and P. Adelhelm, *ACS Appl. Mater. Interfaces*, 2019, **11**, 32844–32855.
112 L. Zhou, Z. Cao, J. Zhang, Q. Sun, Y. Wu, W. Wahyudi, J.-Y. Hwang, L. Wang, L. Cavallo, Y.-K. Sun, H. N. Alshareef and J. Ming, *Nano Lett.*, 2020, **20**, 3247–3254.
113 F. Cheng, M. Cao, Q. Li, C. Fang, J. Han and Y. Huang, *ACS Nano*, 2023, **17**, 18608–18615.

114 P. M. L. Le, T. D. Vo, H. Pan, Y. Jin, Y. He, X. Cao, H. V. Nguyen, M. H. Engelhard, C. Wang, J. Xiao and J.-G. Zhang, *Adv. Funct. Mater.*, 2020, **30**, 2001151.
115 C. Wang, A. C. Thenuwara, J. Luo, P. P. Shetty, M. T. McDowell, H. Zhu, S. Posada-Pérez, H. Xiong, G. Hautier and W. Li, *Nat. Commun.*, 2022, **13**, 4934.
116 J. Zhou, Y. Wang, J. Wang, Y. Liu, Y. Li, L. Cheng, Y. Ding, S. Dong, Q. Zhu, M. Tang, Y. Wang, Y. Bi, R. Sun, Z. Wang and H. Wang, *Energy Storage Mater.*, 2022, **50**, 47–54.
117 A. C. Thenuwara, P. P. Shetty, N. Kondekar, C. Wang, W. Li and M. T. McDowell, *J. Mater. Chem. A*, 2021, **9**, 10992–11000.
118 Q. Zhu, D. Yu, J. Chen, L. Cheng, M. Tang, Y. Wang, Y. Li, J. Yang and H. Wang, *Joule*, 2024, **8**, 482–495.
119 Y. Chen, Z. Yu, P. Rudnicki, H. Gong, Z. Huang, S. C. Kim, J.-C. Lai, X. Kong, J. Qin, Y. Cui and Z. Bao, *J. Am. Chem. Soc.*, 2021, **143**, 18703–18713.
120 C. Heubner, S. Maletti, H. Auer, J. Hüttl, K. Voigt, O. Lohrberg, K. Nikolowski, M. Partsch and A. Michaelis, *Adv. Funct. Mater.*, 2021, **31**, 2106608.
121 M. J. Wang, E. Carmona, A. Gupta, P. Albertus and J. Sakamoto, *Nat. Commun.*, 2020, **11**, 5201.
122 T. Ortmann, T. Fuchs, J. K. Eckhardt, Z. Ding, Q. Ma, F. Tietz, C. Kübel, M. Rohnke and J. Janek, *Adv. Energy Mater.*, 2024, **14**, 2302729.
123 G. Deysher, J. A. S. Oh, Y.-T. Chen, B. Sayahpour, S.-Y. Ham, D. Cheng, P. Ridley, A. Cronk, S. W.-H. Lin, K. Qian, L. H. B. Nguyen, J. Jang and Y. S. Meng, *Nat. Energy*, 2024, **9**, 1161–1172.
124 W. Liu, Y. Luo, Y. Hu, Z. Chen, Q. Wang, Y. Chen, N. Iqbal and D. Mitlin, *Adv. Energy Mater.*, 2024, **14**, 2302261.
125 D. Gu, H. Kim, J.-H. Lee and S. Park, *J. Energy Chem.*, 2022, **70**, 248–257.
126 S. Li, M. Jiang, Y. Xie, H. Xu, J. Jia and J. Li, *Adv. Mater.*, 2018, **30**, 1706375.
127 N. Takenaka, A. Bouibes, Y. Yamada, M. Nagaoka and A. Yamada, *Adv. Mater.*, 2021, **33**, 2100574.
128 Y. Li, F. Wu, Y. Li, M. Liu, X. Feng, Y. Bai and C. Wu, *Chem. Soc. Rev.*, 2022, **51**, 4484–4536.
129 S. Menkin, C. A. O'Keefe, A. B. Gunnarsdóttir, S. Dey, F. M. Pesci, Z. Shen, A. Aguadero and C. P. Grey, *J. Phys. Chem. C*, 2021, **125**, 16719–16732.
130 B. Sayahpour, W. Li, S. Bai, B. Lu, B. Han, Y.-T. Chen, G. Deysher, S. Parab, P. Ridley, G. Raghavendran, L. H. B. Nguyen, M. Zhang and Y. S. Meng, *Energy Environ. Sci.*, 2024, **17**, 1216–1228.
131 L. Lutz, D. Alves Dalla Corte, M. Tang, E. Salager, M. Deschamps, A. Grimaud, L. Johnson, P. G. Bruce and J.-M. Tarascon, *Chem. Mater.*, 2017, **29**, 6066–6075.
132 Z. Wang, H. Yang, Y. Liu, Y. Bai, G. Chen, Y. Li, X. Wang, H. Xu, C. Wu and J. Lu, *Small*, 2020, **16**, 2003268.
133 J. Huang, X. Guo, X. Du, X. Lin, J.-Q. Huang, H. Tan, Y. Zhu and B. Zhang, *Energy Environ. Sci.*, 2019, **12**, 1550–1557.
134 Z. Xu, J. Yang, T. Zhang, L. Sun, Y. Nuli, J. Wang and S. I. Hirano, *Adv. Funct. Mater.*, 2019, **29**, 1901924.
135 M. Han, C. Zhu, T. Ma, Z. Pan, Z. Tao and J. Chen, *Chem. Commun.*, 2018, **54**, 2381–2384.
136 C. Zhu, D. Wu, Z. Wang, H. Wang, J. Liu, K. Guo, Q. Liu and J. Ma, *Adv. Funct. Mater.*, 2023, **34**, 2214195.
137 L. Zhang, C. Tsolakidou, S. Mariyappan, J.-M. Tarascon and S. Trabesinger, *Energy Storage Mater.*, 2021, **42**, 12–21.
138 X. Zheng, H. Fu, C. Hu, H. Xu, Y. Huang, J. Wen, H. Sun, W. Luo and Y. Huang, *J. Phys. Chem. Lett.*, 2019, **10**, 707–714.
139 X. Cheng, D. Li, S. Peng, P. Shi, H. Yu, Y. Jiang and S. Li, *Batteries*, 2023, **9**, 408.
140 N. Mubarak, F. Rehman, M. Ihsan-Ul-Haq, M. Xu, Y. Li, Y. Zhao, Z. Luo, B. Huang and J.-K. Kim, *Adv. Energy Mater.*, 2022, **12**, 2103904.
141 S.-J. Zhang, J.-H. You, Z. He, J. Zhong, P.-F. Zhang, Z.-W. Yin, F. Pan, M. Ling, B. Zhang and Z. Lin, *Adv. Funct. Mater.*, 2022, **32**, 2200967.
142 M. E. Lee, S. Lee, J. Choi, H. J. Jin, S. Han and Y. S. Yun, *Small*, 2019, **15**, 1901274.
143 A. P. Cohn, T. Metke, J. Donohue, N. Muralidharan, K. Share and C. L. Pint, *J. Mater. Chem. A*, 2018, **6**, 23875–23884.
144 Y. Li, M. Chen, B. Liu, Y. Zhang, X. Liang and X. Xia, *Adv. Energy Mater.*, 2020, **10**, 2000927.
145 Y. Gao, T. Rojas, K. Wang, S. Liu, D. Wang, T. Chen, H. Wang, A. T. Ngo and D. Wang, *Nat. Energy*, 2020, **5**, 534–542.
146 Z. Cai, F. Tang, Y. Yang, S. Xu, C. Xu, L. Liu and X. Rui, *Nano Energy*, 2023, **116**, 108814.
147 L. Liu, Z. Cai, S. Yang, Y. Yang, Y. Yao, S. He, S. Xu, Z. Wu, H. Pan, X. Rui and Y. Yu, *Adv. Mater.*, 2025, **37**, 2413331.
148 S. Wu, J. Hwang, K. Matsumoto and R. Hagiwara, *Adv. Energy Mater.*, 2023, **13**, 2302468.
149 J. Chen, Y. Wang, S. Li, H. Chen, X. Qiao, J. Zhao, Y. Ma and H. N. Alshareef, *Adv. Sci.*, 2023, **10**, 2205695.
150 Z. P. Li, K. J. Zhu, P. Liu and L. F. Jiao, *Adv. Energy Mater.*, 2021, **12**, 2100359.
151 E. R. Cooper, M. Li, Q. Xia, I. Gentle and R. Knibbe, *ACS Appl. Energy Mater.*, 2023, **6**, 11550–11559.
152 T.-S. Wang, Y. Liu, Y.-X. Lu, Y.-S. Hu and L.-Z. Fan, *Energy Storage Mater.*, 2018, **15**, 274–281.
153 S.-S. Chi, X.-G. Qi, Y.-S. Hu and L.-Z. Fan, *Adv. Energy Mater.*, 2018, **8**, 1702764.
154 W. Zhang, J. Zheng, Z. Ren, J. Wang, J. Luo, Y. Wang, X. Tao and T. Liu, *Adv. Mater.*, 2024, **36**, 2310347.
155 Y. Yao, Y. Yang, Z. Wang, M. Guo, P. Liu and Z. Xing, *J. Power Sources*, 2024, **613**, 234917.
156 M. Genovese, A. J. Louli, R. Weber, C. Martin, T. Taskovic and J. R. Dahn, *J. Electrochem. Soc.*, 2019, **166**, A3342.
157 A. J. Louli, M. Genovese, R. Weber, S. G. Hames, E. R. Logan and J. R. Dahn, *J. Electrochem. Soc.*, 2019, **166**, A1291.
158 S. E. Sandoval, C. G. Haslam, B. S. Vishnugopi, D. W. Liao, J. S. Yoon, S. H. Park, Y. Wang, D. Mitlin, K. B. Hatzell, D. J. Siegel, P. P. Mukherjee, N. P. Dasgupta, J. Sakamoto and M. T. McDowell, *Nat. Mater.*, 2025, DOI: **10.1038/s41563-024-02055-z**.
159 T. Marks, S. Trussler, A. J. Smith, D. Xiong and J. R. Dahn, *J. Electrochem. Soc.*, 2011, **158**, A51.

160 E. Talaie, P. Bonnick, X. Sun, Q. Pang, X. Liang and L. F. Nazar, *Chem. Mater.*, 2016, **29**, 90–105.
161 C. Zhou, A. J. Samson, M. A. Garakani and V. Thangadurai, *J. Electrochem. Soc.*, 2021, **168**, 060532.
162 J. Cannarella and C. B. Arnold, *J. Power Sources*, 2014, **245**, 745–751.
163 V. Müller, R.-G. Scurtu, K. Richter, T. Waldmann, M. Memm, M. A. Danzer and M. Wohlfahrt-Mehrens, *J. Electrochem. Soc.*, 2019, **166**, A3796.
164 A. Willow, H. E. M. Hussein, S. Vajirakaphan, A. Chasri and S. Margadonna, *Front. Energy Res.*, 2022, **10**, 888321.
165 Y. Xi, X. Ye, S. Duan, T. Li, J. Zhang, L. Jia, J. Yang, J. Wang, H. Liu and Q. Xiao, *J. Mater. Chem. A*, 2020, **8**, 14769–14777.
166 J. Fish, G. J. Wagner and S. Keten, *Nat. Mater.*, 2021, **20**, 774–786.
167 H. Adenusi, G. A. Chass, S. Passerini, K. V. Tian and G. Chen, *Adv. Energy Mater.*, 2023, **13**, 2203307.
168 G. Li and C. W. Monroe, *Annu. Rev. Chem. Biomol. Eng.*, 2020, **11**, 277–310.
169 J. Wang, H. T. Liu, Q. B. Xiao, C. Wang, Y. Z. Zhang, M. A. Liu, Q. Kang, L. J. Jia, D. Wang, Q. Li, W. H. Duan, H. Adenusi, S. Passerini, Y. G. Zhang and H. Z. Lin, *Energy Storage Mater.*, 2024, **67**, 103289.
170 Z. Wu, Y. Zuo, Y. Zhang, X. Li, J. Zhang, Y. Wang, C. Shen, X. Cheng, M. Liu, H. Liu, H. Lin, J. Wang, L. Zhan and L. Ling, *Energy Storage Mater.*, 2024, **70**, 103463.
171 J. Maibach, J. Rizell, A. Matic and N. Mozhzhukhina, *ACS Mater. Lett.*, 2023, **5**, 2431–2444.
172 D. Shanmukaraj, K. Kretschmer, T. Sahu, W. Bao, T. Rojo, G. Wang and M. Armand, *ChemSusChem*, 2018, **11**, 3286–3291.
173 Y. B. Niu, Y. J. Guo, Y. X. Yin, S. Y. Zhang, T. Wang, P. Wang, S. Xin and Y. G. Guo, *Adv. Mater.*, 2020, **32**, 2001419.
174 X. Liu, Y. Tan, W. Wang, P. Wei, Z. W. Seh and Y. Sun, *ACS Appl. Mater. Interfaces*, 2021, **13**, 27057–27065.
175 B. Zhang, R. Dugas, G. Rousse, P. Rozier, A. M. Abakumov and J.-M. Tarascon, *Nat. Commun.*, 2016, **7**, 10308.
176 J. Martinez De Ilarduya, L. Otaegui, J. M. López del Amo, M. Armand and G. Singh, *J. Power Sources*, 2017, **337**, 197–203.
177 H. Yuan, K. Wen, S. Guan, Y. Liang, Y.-H. Wu, S. Liu, D. Yu, L. Li and C.-W. Nan, *J. Materiomics*, 2024, **10**, 643–651.
178 H. Liu, X. Zheng, Y. Du, M. C. Borrás, K. Wu, K. Konstantinov, W. K. Pang, S. Chou, H. Liu, S. Dou and C. Wu, *Adv. Mater.*, 2024, **36**, 2307645.

